Draft version October 29, 2018
Preprint typeset using LaTeX style emulateapj v. 11/12/01

A DEEP CATALOG OF VARIABLE STARS IN A 0.66DEG^2 LUPUS FIELD

David T. F. Weldrake
Max Planck Institut für Astronomie, Königstuhl 17, D-69117, Heidelberg, Germany
weldrake@mpia-hd.mpg.de

Daniel D. R. Bayliss
Research School of Astronomy and Astrophysics, Australian National University, Mount Stromlo Observatory, Cotter Road, Weston Creek, ACT 2611, Australia
daniel@mso.anu.edu.au

Draft version October 29, 2018

ABSTRACT

We have conducted a wide-field photometric survey in a single $52' \times 52'$ field towards the Lupus Galactic Plane in an effort to detect transiting Hot Jupiter planets. The planet Lupus-TR-3b was identified from this work. The dataset also led to the detection of 494 field variables, all of which are new discoveries. This paper presents an overview of the project, along with the total catalog of variables, which comprises 190 eclipsing binaries (of contact, semi-contact and detached configurations), 51 miscellaneous pulsators of various types, 237 long period variables (P$\geq$2d), 11 δ Scuti stars, 4 field RR Lyrae (3 disk and 1 halo) and 1 irregular variable. Our survey provides a complete catalog of W UMa eclipsing binaries in the field to V=18.8, which display a Gaussian period distribution of 0.277$\pm$0.036d. Several binary systems are likely composed of equal mass M-dwarf components and others display evidence of mass transfer. We find 17 candidate blue stragglers and one binary that has the shortest period known, 0.2009d (V=20.9). The frequency of eclipsing binaries (all types) is found to be $1.7\pm0.4\times10^{-3}$ per star, substantially higher (by a factor of 3-10) than previously determined in the haloes of the globular clusters 47 Tuc and ω Cen. This indicates that cluster dynamics aids mass segregation and binary destruction.

Subject headings: binaries: eclipsing — binaries: general — stars: variables: δ Scuti — other

1. INTRODUCTION

The discovery rate of field variable stars has dramatically increased in recent years due to the advent of large-scale photometric surveys with wide fields of view. Many such surveys are dedicated to the detection of transiting short period planets or microlensing events (for example Woźniak et al. (2004) and references there-in). They are perfectly suited to the detection of variable stars (Soszyński 2006; Alcock et al. 2003), as they incorporate long temporal baselines, high resolution imagery, and achieve simultaneous high precision photometry for tens of thousands of stars.

Variable stars provide important information on the frequency, nature and evolution of stellar variability (of all types) in various regions of the Galaxy. Binary stars provide information on stellar mass-radius relationships across many orders of magnitude, particularly for the little-understood relation for the lowest mass stars. Pulsating variables (such as δ Scuti stars) offer insights into the internal structure and evolution of main sequence and post-main sequence objects. RR Lyrae and Cepheids are often used as distance indicators and their identification (particularly in stellar clusters) provides additional distance information for comparing stellar properties with that provided by theoretical isochrones.

Unlike microlensing surveys, transit surveys have temporal resolution of several minutes, permitting the detection of variability on very short time-scales, as well as longer period variability depending on dataset properties. Kane et al. (2005) present an example of a variable star catalog from a wide angle transit survey in the general field, containing the types of variability commony found. Similarly, Weldrake et al. (2004, 2007a) present the variables identified during a transit survey of the haloes of 47 Tucanae (47 Tuc) and ω Centauri (ω Cen). Open clusters have also been targeted (Pepper & Burke 2006 and references there-in) and the Permanent All Sky Survey (Deeg et al. 2004) has the goal of permanently tracking variable stars in the whole sky with high temporal resolution.

This paper presents the total catalog of 494 variable stars identified during a deep, wide single-field survey for transiting Hot Jupiter planets ($\sim$Jupiter-mass planets with orbital periods of a few days) towards the Lupus Galactic Plane. In addition to searching for transiting planets, this survey acts as a control field for our previous 47 Tuc and ω Cen transit surveys, both of which produced significant null results. One object, Lupus-TR-3b, that is almost certainly a transiting low-mass Hot Jupiter has been identified in our survey (Weldrake et al. 2007b). The survey also serves as an excellent test into the techniques and strategies for use in the soon-to-begin 5.7deg^2 SkyMapper transit survey (Bayliss & Sackett 2007). SkyMapper has the capacity to discover dozens of new transiting planets and thousands of variable stars in the near future.

Here we present the properties of all 494 variables, and illustrative V+R lightcurves for the majority of the catalog. We detail a preliminary analysis on their occurrence rates and likely nature, particularly in comparison to previous work in the fields of the globular clusters 47 Tuc and ω Cen (Weldrake et al. 2004, 2007a,c). We find a significant difference in the occurrence rate for binary stars, with our field having three times the observed binary frequency

of ω Cen and ten times that of 47 Tuc. This supports mass segregation, particularly for 47 Tuc, and overall binary destruction in globular clusters due to cluster dynamics. Several of our binary systems are likely composed of M dwarf components, of interest in the study of low mass stars, and several other binaries display evidence of mass transfer, important for studies into binary system evolution and stellar interactions. We have also identified 17 blue straggler candidates and a binary which very likely contains a δ Scuti component.

Section 2 of this paper details the observational strategy and data reduction techniques. Section 3 describes the production of the stellar time-series, the removal of dataset systematics, resulting photometric accuracy, and stellar colors and astrometry. Section 4 details the variability search methods and dataset completeness. Section 5 presents the variable catalog, detailing each main type of variable and provides the derived binary frequency in our field, with a comparison to the globular clusters and distance estimates for our four RR Lyrae stars. We conclude in Section 6.

2. OBSERVATIONS AND DATA REDUCTION

Using the Australian National University 1m telescope at Siding Spring Observatory, a single $54' \times 54'$ Wide Field Imager (WFI) field was observed for 53 nights, 26 contiguous nights in June 2005 and 27 nights in June 2006. The WFI detector consists of a 4×2 array of 2048×4096 pixel back-illuminated CCDs, arranged to produce a total array of $8\text{K} \times 8\text{K}$ pixels. The detector scale is $0.''38$ per pixel at the Cassegrain focus, well matched to the median seeing at the site (mean seeing of $2.2''$) allowing a suitable sampling of the stellar point-spread function (PSF). During the course of this survey, only 7 of the 8 WFI CCDs were operational, resulting in an effective survey field of 0.66 deg^2.

The survey field is a few degrees from the Galactic Plane and is centered at RA=$15^{\rm h}30^{\rm m}36.3^{\rm s}$, DEC=$-42°53'53.0$" (b=11° l=331.5°). The positions of the centers of each individual WFI CCD are seen in Table. 1. This particular field was chosen as it has excellent visibility during the course of the run, it is permanently located away from the moon, it lacks any stars brighter than V$\sim$11 and is a highly crowded field with low dust extinction.

We require a signal-to-noise ratio of $\sim$200 at V=18.0 to adequately recover the transits of Hot Jupiter planets. In order to do this, we used a single broad-band filter covering the combined wavelength range of Cousins V and R to increase the signal-to-noise. We took 5 minute exposures of the field, which with the V+R filter permitted a photon-noise signal-to-noise of $\sim$220 for a 7-day moon for a V=18.5 star in $2''$ seeing. With a full moon this signal-to-noise decreases to $\sim$165. A total of 2201 images of the field were obtained over the course of 53 nights. Given the CCD readout time, pointing and focusing overheads, a mean temporal resolution of 6-7 minutes was achieved within our observing window (typically 9 hours per night in good conditions). This combination of telescope, detector, filter and observational strategy has been previously used successfully to perform a similar search for planetary transits and variable stars in the globular clusters 47 Tucanae and ω Centauri (Weldrake et al. 2004, 2005, 2006, 2007a).

In addition to the V+R imagery, three images in V and three in I were taken with the same telescope and pointing in order to produce the field color magnitude diagram (CMD). Observations in V and I of Mark-A standard stars (Landolt 1992; Stetson 2000) were also taken on the same night for accurate CMD calibration.

Image reduction was carried out using the standard MSCRED routines within IRAF[1]. This included region trimming, overscan correction, bias correction, flat-field correction and dark current subtraction. Low quality images (poor seeing, poor focus, etc) were filtered out, and the resulting dataset used to produce precise, high resolution, photometric time-series for as many stars as possible in the survey field.

3. LIGHTCURVE PRODUCTION

A total of 110,372 stars were identified in our survey field, and for each we produced a photometric time-series using an application of Differential Imaging Analysis (DIA), previously described as the optimal PSF-matching package of Alard & Lupton (1998). This code was subsequently modified by Wozniak (2000) for the detection of microlensing events. We direct the reader to the Wozniak paper for a full description of the code and its application.

By matching the stellar PSF throughout a large image database, the systematic effects resulting from varying atmospheric conditions on the output photometric precision is dramatically reduced. This method allows ground-based observations the best prospects of detecting small-amplitude brightness variations in faint targets. DIA is also one of the optimal photometric methods when sampling fields with a high degree of crowding, as the large number of stars permits a large number of pixels to contain information on any PSF differences, improving the PSF-matching process. Initial stellar flux measurements are made via profile photometry on a template frame, produced via median-combining a number of the best-quality images with small offsets. The flux measurement on this template is used as the zero point of the resulting stellar time series.

Stellar positions were found on a reference image, which contained the best seeing conditions, and all the subsequent data-set images, including the template, were registered. The best PSF-matching kernel was determined, and each registered image was subsequently subtracted from the template, with the residuals generally being dominated by photon noise. Any object in the frame that changed in brightness between the image and the template was recorded as a bright or dark spot in the residual map.

Differential photometry does not automatically produce time-series in magnitude units, rather in differential counts. This is a linear flux unit output in the code from which a constant reference flux (taken from the template image) has been subtracted. In order to convert to a standard magnitude system, the total number of counts for each star was measured using the PSF package of

[1] IRAF is distributed by National Optical Observatories, which is operated by the Association of Universities for Research in Astronomy, Inc., under cooperative agreement with the National Science Foundation.

DAOPHOT within IRAF, with the same images and parameters as used in the DIA code. The total database of output time series were then converted in a standard way into magnitude units via the relation:

$$\Delta m_i = -2.5 \log[(N_i + N_{\mathrm{ref},i})/N_{\mathrm{ref},i}]$$

where $N_{\mathrm{ref},i}$ is the total flux of star i on the template image and N_i is the original difference flux in the time series as produced with the photometric code.

The pixel coordinates of all the visible stars were determined separately from the reference frame via DAOFIND within IRAF, with the resulting profile photometry extracted from the subtracted frames at those determined positions. Due to the filter chosen, the time-series are presented here in V+R differential magnitude units. These can be converted to the standard V system if required via the additional calculation of color terms.

When combining differential fluxes with DAOPHOT-derived photometry on the reference image, we must correct for errors based on the individual apertures used. The scaling between the two fluxes was determined via an aperture correction, which was performed on the DAOPHOT magnitudes for the stars. This method is described in Appendix B of Hartman et al. (2004). We found that our PSF magnitudes were consistently 0.06 magnitudes brighter than the aperture-derived values (using the same aperture values as in the differential photometry). We corrected for this by shifting our magnitude zero-point to 25.0−0.06=24.94. This correction ensures that the amplitude of moderate variation detected by the DIA code is accurately represented in magnitude units.

3.1. *Systematics Removal and Photometric Accuracy*

All 110,372 time-series as output by DIA were converted to ΔV+R magnitude units as above. The whole dataset was cleaned for systematic effects by running an application of the SYSREM systematics removal code (Tamuz et al. 2005). This algorithm searches for and removes effects common to the stars of a particular dataset, using only the time of observation and the respective flux measurements for all stars simultaneously. The result is a dramatic increase in the photometric precision, of vital importance to any search for small amplitude brightness variations. The algorithm works best for brighter stars, where systematic effects dominate in the photometric uncertainties.

Fig. 1 presents the output DIA-derived photometric precision for 90,959 stars across the whole of the WFI field, after an application of the SYSREM algorithm. These stars are those for which both a post-SYSREM lightcurve, V magnitude and astrometry have been derived. The V magnitudes for these stars were determined from the field color-magnitude diagram (see next subsection). The Y-axis shows the logarithm of the measured root-mean-square (*rms*) uncertainty for the whole stellar lightcurve, plotted against the V magnitude of the same star. Some variable stars are visible as a separate sequence above the main *rms* distribution (particularly for brighter stars). Also overplotted on the figure is the theoretical photon noise due to the star (green short-dashed line) and the sky noise contribution (blue long-dashed line). A further noise contribution arises from residual image-based systematic effects; flat-fielding errors, scintillation and CCD non-linearity response. All of these are estimated with an amplitude of four times the calculated sky noise to represent the total observed noise when added to the photon noise in the star and the sky, and is displayed on Fig. 1 as a dash-dotted blue line. The solid red line represents the total of the photon noise and this total sky contribution (added quadratically), and describes the photometric uncertainties well. Our photometry is photon-noise dominated to a V magnitude of ∼18.5, where it becomes sky+residuals dominated to fainter magnitudes.

3.2. *Color-Magnitude Diagram and Astrometry*

A color-magnitude diagram (CMD) of V−I against V was produced for the survey field with the same telescope and detector, in order to place the detected variables (and transit candidates) onto the standard magnitude system. The diagram contains a total of 95,358 stars with both measured V and I magnitudes. This CMD, with all 494 detected variables overplotted, can be seen in Fig. 2. The figure shows four panels, one for each of the main type of variable star found (overplotted). The four main types can be seen to populate different regions of the CMD, depending on their intrinsic spectral type. Our survey has a saturation limit at V=15.0, and a faint limit of V=22.0. A sharp edge is seen at V−I=0.6, indicating the Galactic disk main sequence turn-off, the limit of the more numerous F,G,K and M stars (to the right of the edge) compared to the far less numerous earlier type stars (to the left of the edge) at the typical age of the galactic disk. The DAOPHOT-derived errors and calibration uncertainty in our magnitude determinations are also overplotted.

The CMD was calibrated via V and I observation of the MarkA standard stars (Landolt 1992; Stetson 2000), taken at the same time as the CMD data. A total of 415 standards were cross-identified in the field via matching of astrometry[2]. The mean and standard deviation of the shift in magnitude was found for each CCD and for each filter independently. The resulting calibration uncertainty is 0.03 magnitudes in V and 0.05 in V−I. As an additional check, the CMD was also cross-correlated with 2,000 stars within 20′ of the field center in the NOMAD online catalog (Zacharias et al. 2004), and, being towards the faint limit of NOMAD, have V magnitudes within 0.2 magnitudes (1σ) of the NOMAD results.

The astrometry for all of the stars in our database was determined via a search of the USNO CCD Astrograph Catalog (UCAC1), to search for astrometric standard stars within the field. Several hundred such stars were successfully identified, producing an accurate determination of the astrometric solution for the stars in each CCD independently; the resulting calibration accuracy was 0.25″ (0.66 pixels). The extent of our field can be seen in Fig. 3, plotted as ΔRA and ΔDec in degrees. The location of the variable stars are overplotted with the same color scheme as in Fig. 2. The non-functioning WFI CCD7 is clear.

4. VARIABILITY SEARCH METHOD AND COMPLETENESS

[2] MarkA astrometry and photometry downloaded from http://www4.cadc-ccda.hia-iha.nrc-cnrc.gc.ca/community/STETSON/standards/

We used the 'analysis of variance' (AoV) statistic to perform the variability search, with Schwarzenberg-Czerny (1989) providing a full description of the method. Via AoV, the data are phase-wrapped to a trial period and grouped into phase bins. A one-way statistical analysis of variance is performed on the result with the output noted. This procedure is repeated for a fixed range of test periods for each star, producing a series of significances and their corresponding periodicities. The final output for each star is the peak periodicity and its corresponding significance.

The output AoV significance is far higher if a periodicity is detected, facilitating the variable identification, and allowing for detection thresholds to be used to increase the search efficiency. Fig. 4 shows the output AoV significance (S_{AoV}) distribution for the whole time-series dataset. The main population at low significances are those stars for which no periodicity was detected. The variable star candidates constitute the long tail to increasingly higher significance. The main population was fit with a Gaussian, overplotted in Fig. 4 with a resulting mean S_{AoV} =3.904 and standard deviation (*rms*) of S_{AoV} =0.499.

Any candidate with a significance $\geq 3\times rms$ (9,230 candidates $S_{AoV}\geq 5.401$) was counted as a candidate variable star, which was then phase-wrapped at the AoV determined peak periodicity and the presence of any variability noted. This candidate detection threshold is marked in Fig. 4 with a vertical line.

We visually searched through all 9,230 candidates to detect the variable stars, which were also phase-wrapped to 0.5, 2 and 3 times the detected period to check for the presence of integer aliasing. Out of these, we visually detected a total of 572 variables, corresponding to one real variable per 16.1 candidates. With such a large number, the chance of any real variables being missed in the search and escaping detection via this method is low.

The total candidate list numbered 572 stars that were seen to undergo periodic brightness changes, 77 more than the final variable list. The astrometry for the original 572 were checked for double entries, consisting of candidates that lie within several arcseconds of each other in both RA and DEC, and also variables with the same or very similar ($\leq$0.1d) peak periodicity. The majority of the extra 77 were found to be double entries, particularly comprised of fainter 'variables' which lie close ($\leq 5''$) to a far brighter real variable. We classify these as 'blends', and have lightcurves with the same periodicity as the bright nearby variable, but with only a fraction of the signal. The RR Lyrae stars, being so bright, were particularly responsible for these blended candidates. The remaining few false variables were identified by their common periods to more distant, yet still nearby, bright counterparts. In all, 494 true variables remained in the candidate list and constitute the final catalog.

A small number of the detected variables ($\sim$5%) had significant scatter on the resulting phase-wraps, indicating an incorrect determination of the period. These were then analyzed with a Lomb-Scargle Periodogram (Bretthorst 2001) to provide a secondary estimate to the period. This was then phase-wrapped and the period optimized until a minimum in the scatter was obtained. The change in period needed to obtain the final period was less than 0.1d in all cases, and is related to the number of datapoints contained within the periodicity. The small number of these statistical false-period detections is further evidence of the strength of AoV as an accurate periodicity determinator.

Fig. 5 presents the total amplitude of the variation for each cataloged variable star, plotted as a function of its corresponding V magnitude. This provides information on the detection limits of the catalog. The dotted line defines the observed empirical limit in the variable amplitude as magnitude increases. Any variable with an amplitude less than or equal to the position of the dotted line is unlikely to be revealed by the detection method described above. Hence, at V=18.0, the observed detection limit is 0.05 magnitudes (4.7%), while at V=22.0, the limit is 0.70 magnitudes (91%), and originates from our photometric uncertainties (Fig. 1).

5. VARIABLE STAR CATALOG

In total the catalog contains 494 variable stars. This consists of 190 eclipsing binary (EcB) systems, displaying many examples of detached (eg: V8), semi-detached (eg: V26) and contact (eg: V3,) configurations. It also contains 51 pulsating stars (puls) defined as having a sinusoidal variation and period $\leq$2d; and 237 long period variables (LPV), which display similar variation to the pulsators but with far longer periods ($2 \leq P \lesssim 100$d). We also detected 11 δ Scuti stars with extremely short pulsation periods (minutes in many cases) and 4 field RR Lyrae stars (three type 'AB' and one type 'C'). We also detected a single irregular variable. The lightcurve database is available on the online edition of this paper.

The total variable star catalog (in order of RA) can be seen in Table 2. This table presents the identification number of the variable, the type of variability (tabulated in order of type: EcB, RR Lyrae, δ Scuti, puls, LPV and Irr), the period in days, the RA and DEC (J2000.0), the V magnitude, V uncertainty and finally the V$-$I color and associated error. The V magnitude, uncertainty and V$-$I color are all taken from the color magnitude diagram dataset. The uncertainties include calibration errors. If a particular binary has an orbital period $\leq$0.385d (from the determined 3σ lower limit to their period distribution, see later) we classify it as a W UMa type system, and is marked as such in the table. Those magnitudes marked with '$-$' have unknown magnitude in that particular band, the vast majority of which are due to saturation in one filter.

Accurately determined periods are presented to five decimal places. Variables with less certain periods are presented with a number of decimal places appropriate to the uncertainty. Those pulsating variables which could in reality be short-period eclipsing binaries, indistinguishable in our data, with equal-mass components W Ursae Majoris (W UMa) stars, and hence identical primary and secondary eclipses, have their periods marked with an asterisk. Those longer period variables and binaries with only one single eclipse visible (hence uncertain periods) have their estimated periods presented, which are marked with a '$\sim$'. Those variables classed as pulsators which could be actually eclipsing binaries with twice the tabulated period are marked with a '$*$'.

The total catalog of variables is overplotted on the dataset CMD in the four panels of Fig. 2, to facilitate de-

termination of their likely nature. The EcB stars (top left, blue squares) are seen to inhabit all parts of the diagram, indicating the differing component spectral types and distances to these systems. In contrast the δ Scuti stars (bottom left, yellow circles) and RR Lyrae (bottom left, green triangles) are all located blueward of the main 'shoulder' seen at V−I=0.6. This indicates that these types of variability are associated exclusively with stars of earlier spectral types ($\leqslant$A-F). No faint δ Scuti stars were seen in our data, due to the low amplitude of their variability. In comparison, all but two of the LPV (V200 and V401) (red triangles) are located redward of the V−I=0.6 shoulder, indicating the association of this type of variability with later spectral types ($\geqslant$G−M). All but four of the pulsators (bottom right; V291, V319, V338 and V491) are located red-ward of V−I=0.5.

5.1. *Eclipsing Binaries*

A total of 190 EcB systems were found in our data. These include many examples of contact, semi-detached and detached systems. The vast majority of the binaries have accurate periodicities determined, with the exception being those long period fully detached systems with only one or two eclipses visible during our observing run. We classify those 17 binaries blue-ward of V−I=0.5 (V36, V44, V76, V113, V117, V168, V228, V253, V257, V294, V296, V317, V385, V405, V442, V467 and V476 as seen in Fig. 2) as candidate blue-stragglers. Particularly, V385, V405 and V467 have 'blue' V−I magnitudes of 0.244, 0.272 and 0.253 respectively. Some binaries (for example V10 and V31) are difficult to phase-wrap accurately, due to the low number of eclipses visible in our data.

5.1.1. *Selected Binary Systems*

Several of our binary systems are of particular interest for follow-up studies. V413 is the brightest binary detected in this search, with V=14.595±0.008 and orbital period 1.7962d. The total phase-wrapped lightcurve for this semi-detached system is seen within Fig. 14 and in greater detail in Fig. 6. It displays a very deep primary eclipse (ΔV+R$\sim$2 mags) and a far shallower secondary eclipse. This indicates that the two stellar components are of very different spectral types and luminosities.

Closer examination of the V413 lightcurve reveals a secondary pulsation variation with a period of only a few minutes, typical of a δ Scuti star. The amplitude of this pulsation is $\geqslant$5 mmag and can be seen in both panels of Fig. 6 (phase-wrapped in the bottom panel to 5 times the periodicity for ease of visibility). Such variations indicate the presence of a small-scale surface variability similar to solar surface oscillations. The period of this secondary oscillation is comparable to the exposure time of the observations, hence the amplitude presented here carries uncertainty. Furthermore, the period of this oscillation is seemingly $1/500^{\rm th}$ the binary orbital period, perhaps indicating that it may originate with surface jitter induced by the binary companion. A second theory, and perhaps more likely, is that one component of this binary is a δ Scuti star. Follow-up photometry and spectroscopy are planned to fully understand this interesting system.

V161 displays a long period sinusoidal variation with a superimposed eclipse with the same period. The system is quite red (V−I=0.96) and is perhaps composed of a pulsating red variable, which is in turn orbited by a stellar companion. Alternatively the system could contain a red giant which has been significantly distorted by a nearby massive companion.

As our survey field was observed for 27 nights in June 2005 and 26 nights in June 2006, changes in any variability during the course of that year can be seen in our lightcurves. V130 (orbital period 1.22086d) displays a consistent change in system brightness (out-of-eclipse zero-point) of $\sim$0.1 mags (V+R) during this time, the system is brighter in 2007. This can be seen in the phase-wrapped lightcurve for this system in Fig. 9. We attribute this variation to one component being a long period variable in itself. As the change is stable over the course of a month, we cannot attribute this to starspots or flare activity. If the components are interacting with each other, as the out-of-eclipse ellipsoidal variations seem to indicate, then an accretion scenario may be present in this system.

A number of our binaries are likely composed of low-mass M-dwarf components, as such they are of importance to studies of stellar mass and radius relationships for late-type stars. These systems were chosen based on their V magnitude and V−I color, along with their short orbital periods and the evidence for only a small degree of interaction between the components in their lightcurves. We classify V26, V115, V184, V297, V304, V352, V355, V402, V418 and V438 as likely low-mass systems. Particularly interesting are V304 and V402 as detached systems. V232 is extremely faint (V=21.99) with a V−I of 2.91, and is almost certainly composed of very low-mass stars.

A number of the longer period systems could also contain a low-mass component again based on the amplitude of gravity effects and the difference in primary and secondary eclipse depths (for example V144 and V312). Indeed, the systems classified as W UMa stars (seen in Table. 2) almost certainly contain low-mass components. Interestingly these W UMa stars are seen as mostly blue straggler systems in old globular clusters (Weldrake et al. 2004, 2007a) rather than late-type stars expected for the (younger) general field. The shortest period binary detected in this survey is V344, with an orbital period of 0.2009 days (V=20.9), and if confirmed will become the shortest period binary known (beating shorter than the previous 0.215d binary found in 47 Tuc by Weldrake et al. 2004).

5.1.2. *Eclipsing Binary Period Distribution*

Fig. 7 displays the *n(P) dP* eclipsing binary period distribution, to an maximum limit of 1d, which contains all the binaries we define as contact binaries. The number of binaries can be seen to generally increase as period decreases, with a population of binaries centered at a period of $\sim$0.27d. We define these as the W Uma systems, short period equal-mass contact binaries that make up the most commonly observed type of field binary (L.Kiss, private communication).

Given the very short periods of these systems ($\sim$0.27d), the total length of our observing window (53 nights or 100 times the typical orbital period assuming a night is 0.5d long), and the considerable amplitude of these systems ($\geq$0.1 magnitudes), we conclude that all systems with suit-

able inclination to undergo eclipses will have been detected in our field down to a magnitude of V=18.8, as determined from our photometric uncertainties (Fig. 1) and our total catalog completeness limits (Fig. 5). They do not suffer in any significant way from detection-related bias. We take the Gaussian appearance of our W Uma period distribution as further evidence of its completeness.

We find a best-fitting Gaussian (via least-squares residuals) to our W UMa population (overplotted on Fig. 7) to have a mean orbital period of 0.277d with associated standard deviation 0.036d. This result compares very well to the 0.27d mean volume-limited W UMa period as determined by Rucinski (2007), from field binaries in the All Sky Automated Survey. We hence determine the 3σ lower limit to our W UMa periods to be 0.17d. Our shortest period binary is 0.2009 days, and is 2.1σ below our mean. W UMa binaries with a period equal to or less than this are exceedingly rare.

5.1.3. *Binary Frequencies and comparison to Globular Clusters*

In the haloes of the globular clusters 47 Tuc and ω Cen, Weldrake et al. (2004, 2007a) determined an observed eclipsing binary frequency of $1.7\pm0.4\times10^{-4}$ and 5.3×10^{-4} respectively (the cluster cores are saturated). The value for 47 Tuc is substantially lower than that observed in the cluster core (Albrow et al. 2001), and this has been taken as evidence for mass segregation in 47 Tuc. Binary destruction due to cluster dynamical processes would produce a substantially higher binary frequency in the general Galactic field.

In our Lupus field, we determine an eclipsing binary frequency of $190/110372=1.7\pm0.4\times10^{-3}$, with the error being 3σ, derived from the Poisson error in both the binary and total star number and applied with standard quotient error propagation. This equates to one detected binary per $\sim$600 stars, ten times the value for 47 Tuc and three times the value for ω Cen.

This strengthens the argument that binaries are less common (particularly long period detached binaries) in the outskirts of globular clusters, being mainly due to mass segregation, and also due to binary destruction. Mass segregation is not thought to be prevalent in ω Cen (which has three times the observed binary frequency of 47 Tuc, yet only $1/3^{rd}$ that of our Lupus field). All three surveys contain a similar total number of stars (within 10%) and have very similar detection thresholds, due to similar global dataset properties. Clearly, the general galactic field contains a higher rate of detectable binary stars than is contained within the haloes of these two globular clusters.

5.2. *δ Scuti and RR Lyrae stars*

A total of 11 δ Scuti stars and four RR Lyrae stars (three type 'AB' and one type 'C') were detected in our data. The δ Scuti stars (also known as a Dwarf Cepheids, AI Velae stars or AI Velorum stars) undergo both radial and non-radial pulsations on short timescales. They were classified as such in this work from their pulsating nature, bluer V−I values and very short periods. The tabulated data for these variables can be seen in Table. 2 and their lightcurves are presented in Fig. 15.

The determined periods range from 0.003919d (V459, 5.6 minutes) to 0.08953d (V270, 2.1 hrs). They (along with the RR Lyrae) are located blueward of the main stellar type 'shoulder' seen in Fig. 2, indicating their classification as stars of earlier spectral type (typically A to F). The moderate amplitude of the V459 pulsation precludes it from being composed of solar-like convection-driven surface oscillations. From the total stellar database of 110,372 stars, we estimate an apparent δ Scuti occurrence frequency in our field of $11/110{,}372=10.0\pm0.3\times10^{-5}$. This corresponds to one δ Scuti per 212 arcmin^2.

RR Lyrae are pulsating horizontal branch stars, that are generally old and with relatively lower mass ($\sim0.8M_{\odot}$). Their identification in the field (particularly in large field surveys targeting the Galactic halo) is important to trace the extent of halo streams. Three of the four detected here are very likely disk stars, due to their apparent brightness, and have pulsation periods and lightcurve shapes typical of the two main classes of RR Lyrae (Vivas et al. 2001). Similarly their data are presented in Table. 2 and Fig. 13. None show evidence of the little understood Blahzko Effect (Blazhko 1907). We estimate an apparent occurrence frequency of $4/110{,}372=3.6\pm0.1\times10^{-5}$ ($\sim$1 RR Lyrae per 583 arcmin^2) for field RR Lyrae towards Lupus. None of the rare AHB RR Lyrae (Sandage, Diethelm, & Tammann 1994) were seen in our data.

RR Lyrae are a well known class of variable due to their usefulness as distance indicators, however their absolute magnitude depends on their metallicity (Sandage 1981a,b). From studies of RR Lyrae and horizontal branch stars in the Milky Way, the LMC and M31 clusters this relation has been adopted with a slope 0.20-0.23 mag/dex (Clementini et al. 2003; Cacciari & Clementini 2003; Gratton et al. 2004). Rich et al. (2005) adopted a relation of the form $M_V=0.20\pm0.09[Fe/H]+0.81\pm0.13$, which was also used to estimate the distance to ω Cen by Weldrake et al. (2007a). The metallicity must be determined spectroscopically before the distance can be estimated with any certainty.

However, if we assume solar metallicity ([Fe/H]=0) for all four RR Lyrae, using the relationship above we determine an absolute V magnitude of 0.81 ± 0.22. By applying the maximum degree of reddening for the field (E(B−V)=0.182 mag (Schlegel et al. 1998)), the V magnitudes of the stars would be altered by $V_{obs}-3.315*E(B-V)$. Hence for the four RR Lyrae and their corresponding V magnitudes (V_{obs}) as listed in Table. 2, we derive minimum reddening-corrected apparent V magnitudes of 14.602 ± 0.003, 15.063 ± 0.002, 14.907 ± 0.002 and 17.146 ± 0.005 for the four stars.

We determine distance modulus $(m-M)_0$ upper limits of 13.80 ± 0.22, 14.25 ± 0.22, 14.10 ± 0.22 and 16.34 ± 0.22 ($\sim$5.7, $\sim$7.0, $\sim$6.6 and $\sim$18.5 Kpc) for our four RR Lyrae, with equal uncertainties throughout as they are strongly dominated by the uncertainty in the absolute magnitude. The faintest RR Lyrae (V387) is likely a background Halo star. Actual metallicity measurements will permit more accurate distances for these stars, rather than the upper limits presented here.

5.3. *Miscellaneous Pulsators*

Our catalog also contains 51 pulsating stars of various types and one irregular variable. We define the pulsators are stars displaying regular pulsation brightness variations with periods less than two days. The global properties of these stars are presented in Table. 2, and the lightcurves for the first 20 pulsators (for illustrative purposes, as visually they appear very similar) can be seen in Figs. 16-17. Longer period pulsators are classified here as long period variables (see below). Their position on the CMD is mostly scattered (Fig. 2) although the majority are quite red, indicating their makeup as later spectral types. The irregular variable (V134) is quite blue (V−I=0.35) indicating it likely is of A-F spectral type and may contain both radial and non-radial pulsations. Their apparent occurrence frequency is $4.6\pm0.3\times10^{-4}$ (one pulsator for every 46 arcmin^2).

The majority of the pulsators display regular radial sinusoidal variations, with periods in the range 0.4→0.6 d, with the lowest being 0.12377d (V238). We classify them as 'pulsators', or red variables, being stars passing through the instability strip during their later evolution. V295 has a period of only 0.04159d, a typical period for a δ Scuti star, however the V−I color is 0.932, unusually red for a δ Scuti, hence its inclusion here.

5.4. *Long Period Variables*

We also detected a total of 237 long period variables (LPVs), by far the most common type of variable seen in our Lupus field, with an observed occurrance frequency of $2.2\pm0.3\times10^{-4}$ (one LPV per 10 arcmin^2). We define these as displaying regular sinusoidal (or slightly sawtooth) variations with various periodicities greater than an arbitrarily chosen lower limit of two days. The global properties of these stars are also seen towards the end of Table 2. The LPVs are in the vast majority very red stars, indicating their likely nature as red giant stars of late spectral types. The lightcurve data themselves can be accessed as online data.

Many of the periods presented in Table. 2 are uncertain, and marked appropriately with a '∼'. This is due to the limitations imposed by our 53-night dataset, variables with significantly longer periods (Mira variables) would be flagged as variable but have indeterminate final periods. Further photometry spanning a long baseline (months) is needed to determine accurate periods for these stars, and is outside the scope of the this project. The lightcurve data (in ASCII format) for all 494 variables in the catalog are available on the on-line edition of the Journal.

6. CONCLUSIONS

We present a variable star catalog, along with a preliminary analysis of the stars, detected during a long-baseline (53 nights: 26 contiguous nights in June 2005 and 27 in June 2006) high temporal resolution (6-7 minutes) photometric survey to detect transiting short period planets towards Lupus. A total of 494 variable stars were detected in our 0.66 deg^2 field, all of which are new discoveries. The catalog comprises 190 eclipsing binaries (of contact, semi-detached and detached configurations), 51 miscellaneous pulsators, 237 long period variables, 11 δ Scuti stars, 4 field RR Lyrae and a single irregular variable.

We determine a period distribution of 0.277±0.035d for our detected short period W UMa binaries (to V=18.8). Several binaries appear to be composed of equal-mass M-dwarf components, and others display evidence of mass transfer. We detected 17 candidate blue straggler stars and we also detected a binary with period 0.2009d (V=20.9), which constitutes the shortest period eclipsing binary known. Our brightest binary likely harbors a δ Scuti component.

We have used this catalog to determine the occurrence frequencies of the various types of variable in our field, and compared the overall frequency of detected binary stars to that previously determined for the haloes of the globular clusters 47 Tuc and ω Cen. We find that the frequency of binary stars is significantly larger in our field than that found in either cluster (ten times for 47 Tuc and three times for ω Cen). This favors the scenario in which binaries are readily mass segregated into the cluster cores and/or destroyed by cluster dynamical processes.

ACKNOWLEDGMENTS

The Authors wish to thank the following people for their assistance during this work: Penny Sackett, Brandon Tingley, Grant Kennedy and Karen Lewis for their help with various aspects of this survey, and Laszlo Kiss for helpful discussion on W UMa stars. We also thank the anonymous referee for their detailed and helpful comments in improving this manuscript.

REFERENCES

Alard, C. & Lupton, R. H. 1998, ApJ, 503, 325
Albrow, M. D., Gilliland, R. L., Brown, T. M., Edmonds, P. D., Guhathakurta, P., & Sarajedini, A. 2001, ApJ, 559, 1060
Alcock, C., et al. 2003, ApJ, 598, 597
Bayliss, D. D. R., & Sackett, P. D. 2007, Transiting Extrasolar Planets Workshop, 366, 320
Blazhko, S. 1907, Astron. Nachr., 175, 325
Bretthorst, G. L. 2001, AIP Conf. Proc. 568: Bayesian Inference and Maximum Entropy Methods in Science and Engineering, 568, 241
Cacciari, C., & Clementini, G. 2003, LNP Vol. 635: Stellar Candles for the Extragalactic Distance Scale, 635, 105
Clementini, G., Gratton, R., Bragaglia, A., Carretta, E., Di Fabrizio, L., & Maio, M. 2003, AJ, 125, 1309
Deeg, H. J., Alonso, R., Belmonte, J. A., Alsubai, K., Horne, K., & Doyle, L. 2004, PASP, 116, 985
Gratton, R. G., Bragaglia, A., Clementini, G., Carretta, E., Di Fabrizio, L., Maio, M., & Taribello, E. 2004, A&A, 421, 937
Hartman, J. D., Bakos, G., Stanek, K. Z., & Noyes, R. W. 2004, AJ, 128, 1761
Kane, S. R., Lister, T. A., Collier Cameron, A., Horne, K., James, D., Pollacco, D. L., Street, R. A., & Tsapras, Y. 2005, MNRAS, 362, 117
Landolt, A. U. 1992, AJ, 104, 340
Pepper, J., & Burke, C. J. 2006, AJ, 132, 1177
Rich, R. M., Corsi, C. E., Cacciari, C., Federici, L., Fusi Pecci, F., Djorgovski, S. G., & Freedman, W. L. 2005, AJ, 129, 2670
Rucinski, S. 2007, ArXiv Astrophysics e-prints, arXiv:astro-ph/0708.3020
Sandage, A. 1981, ApJ, 244, L23
Sandage, A. 1981, ApJ, 248, 161
Sandage, A., Diethelm, R., & Tammann, G. A. 1994, A&A, 283, 111
Schlegel, D. J., Finkbeiner, D. P., & Davis, M. 1998, ApJ, 500, 525
Schwarzenberg-Czerny, A. 1989, MNRAS, 241, 153
Soszyński, I. 2006, Memorie della Societa Astronomica Italiana, 77, 265
Stetson, P. B. 2000, PASP, 112, 925
Tamuz, O., Mazeh, T., & Zucker, S. 2005, MNRAS, 356, 1466
Vivas, A. K., et al. 2001, ApJ, 554, L33

Weldrake, D. T. F., Sackett, P. D., Bridges, T. J., & Freeman, K. C. 2004, AJ, 128, 736
Weldrake, D. T. F., Sackett, P. D., Bridges, T. J., & Freeman, K. C. 2005, ApJ, 620, 1043
Weldrake, D. T. F, Sackett, P. D, & Bridges, T. J 2006, ArXiv Astrophysics e-prints, arXiv:astro-ph/0612215
Weldrake, D. T. F., Sackett, P. D., & Bridges, T. J. 2007a, AJ, 133, 1447
Weldrake, D. T., Sackett, P. D, Bridges, T. J, & . 2007c, ArXiv e-prints, 710, arXiv:0710.3461
Weldrake, D. T. F., Bayliss, D. D. R., Sackett, P. D., Tingley, B. W., Gillon, M., & Setiawan, J. 2007b, ArXiv e-prints, 711, arXiv:0711.1746
Woźniak, P. R., et al. 2004, AJ, 127, 2436
Wozniak, P. R. 2000, Acta Astronomica, 50, 421
Zacharias, N., Monet, D. G., Levine, S. E., Urban, S. E., Gaume, R., & Wycoff, G. L. 2004, Bulletin of the American Astronomical Society, 36, 1418

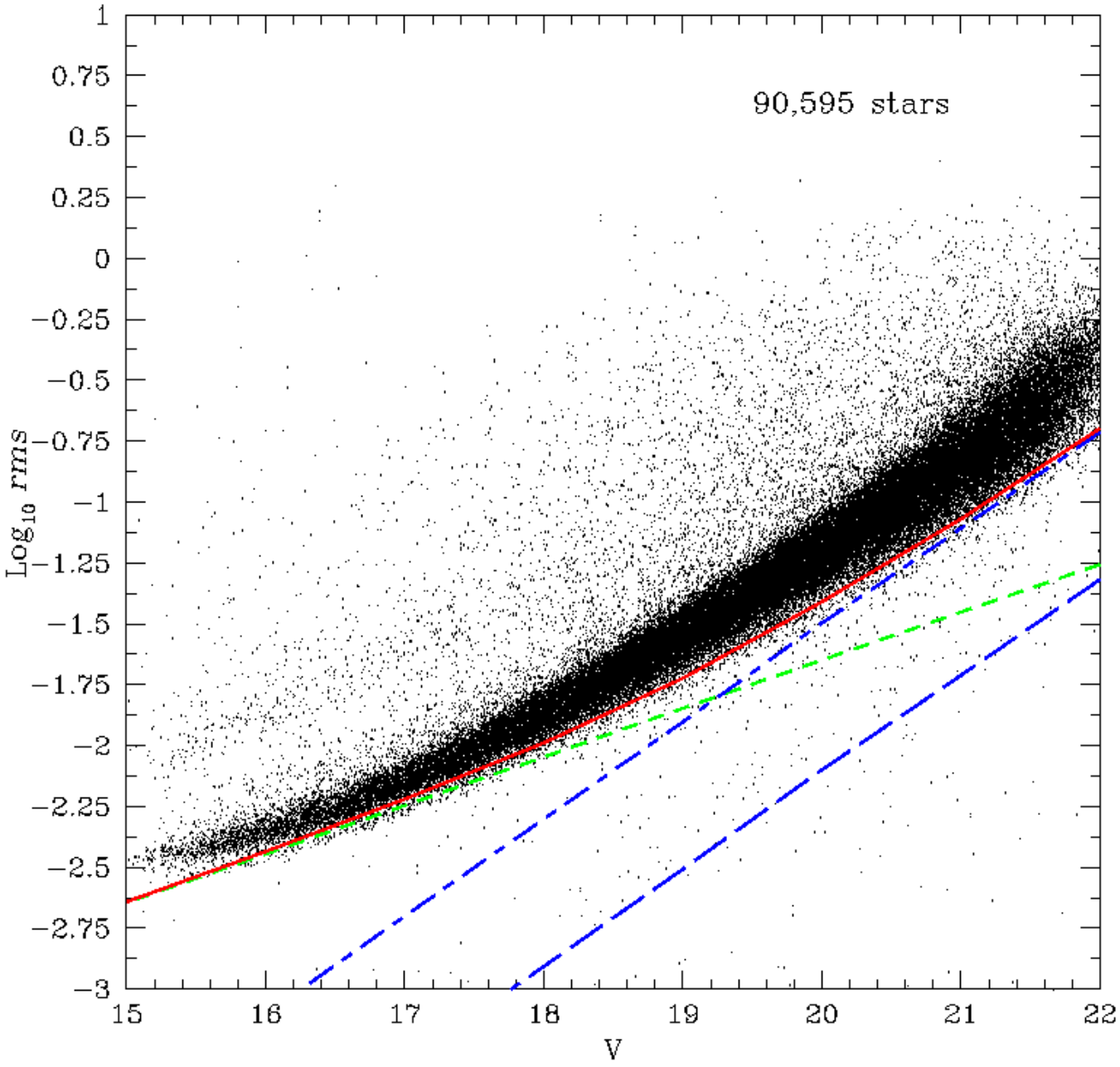

FIG. 1.— The photometric precision of 90,959 stars across the field resulting from the DIA+SYSREM photometry technique applied to our dataset, plotted against V magnitude. The theoretical photon noise for the star (green short-dashed), the sky (blue long-dashed), the residual noise contribution (blue dot-dashed) and the sum of all (red solid line) are overplotted for comparison. Some variable stars are visible as the sequence of higher *rms* at bright magnitudes.

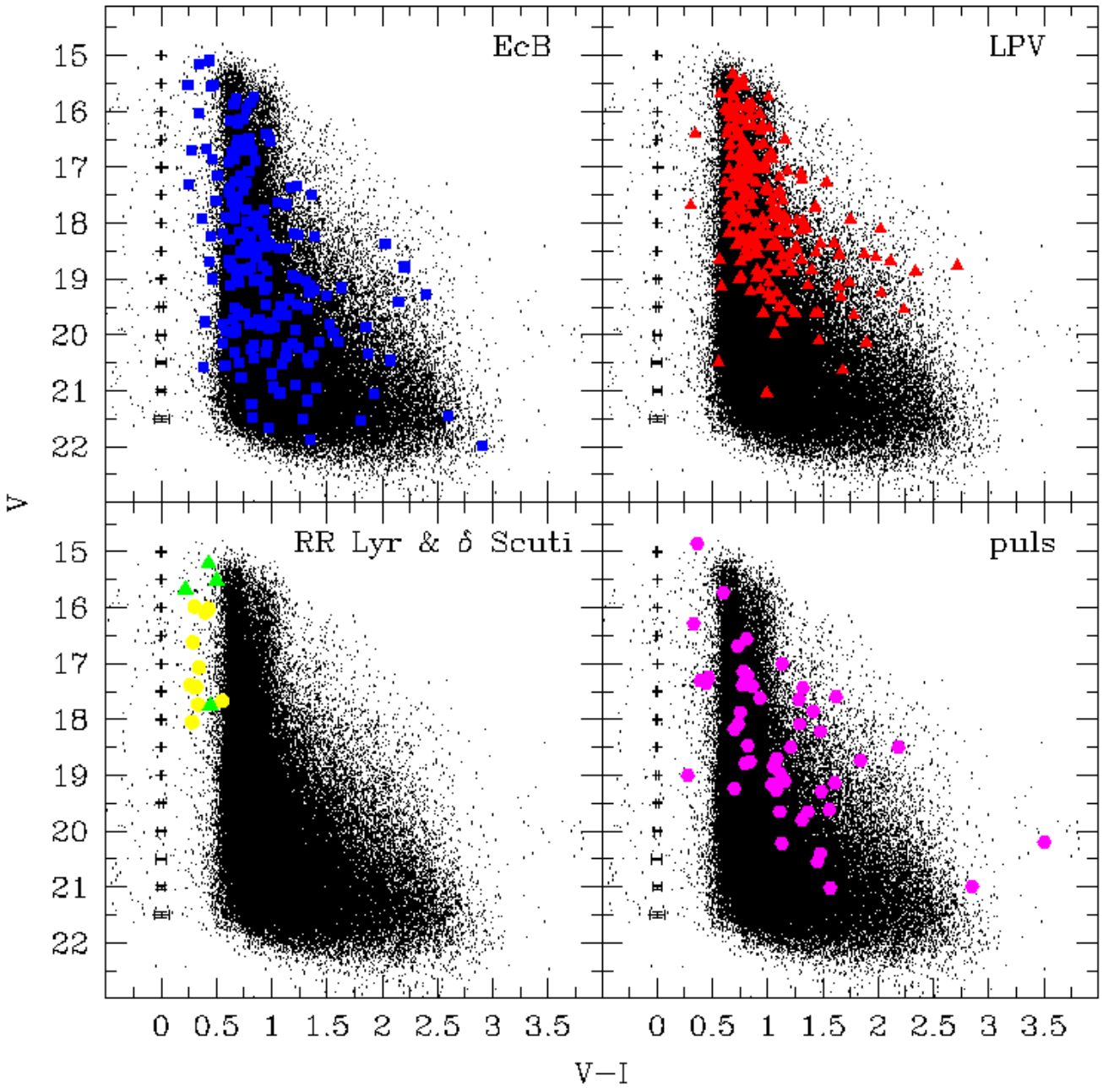

FIG. 2.— The Color-Magnitude Diagram (CMD) for our Lupus field. The locations of all 494 detected variable stars are overplotted. The four panels denote the four main types of variable in the catalog, plotted in various colors to facilitate their visibility. The various types of variable are seen to populate various regions of the CMD. The δ Scuti (yellow) and RR Lyrae stars (green) are all blue-ward of the main shoulder defining the limit of A-F type Galactic Disk stars, indicating their early spectral types. The EcB are scattered all over the plot, indicating the different spectral types of the stellar components. The 17 binaries with V−I values $\leq$0.5 are candidate blue stragglers. The overplotted errorbars represent the output DAOPHOT errors and the CMD calibration uncertainty added in quadrature.

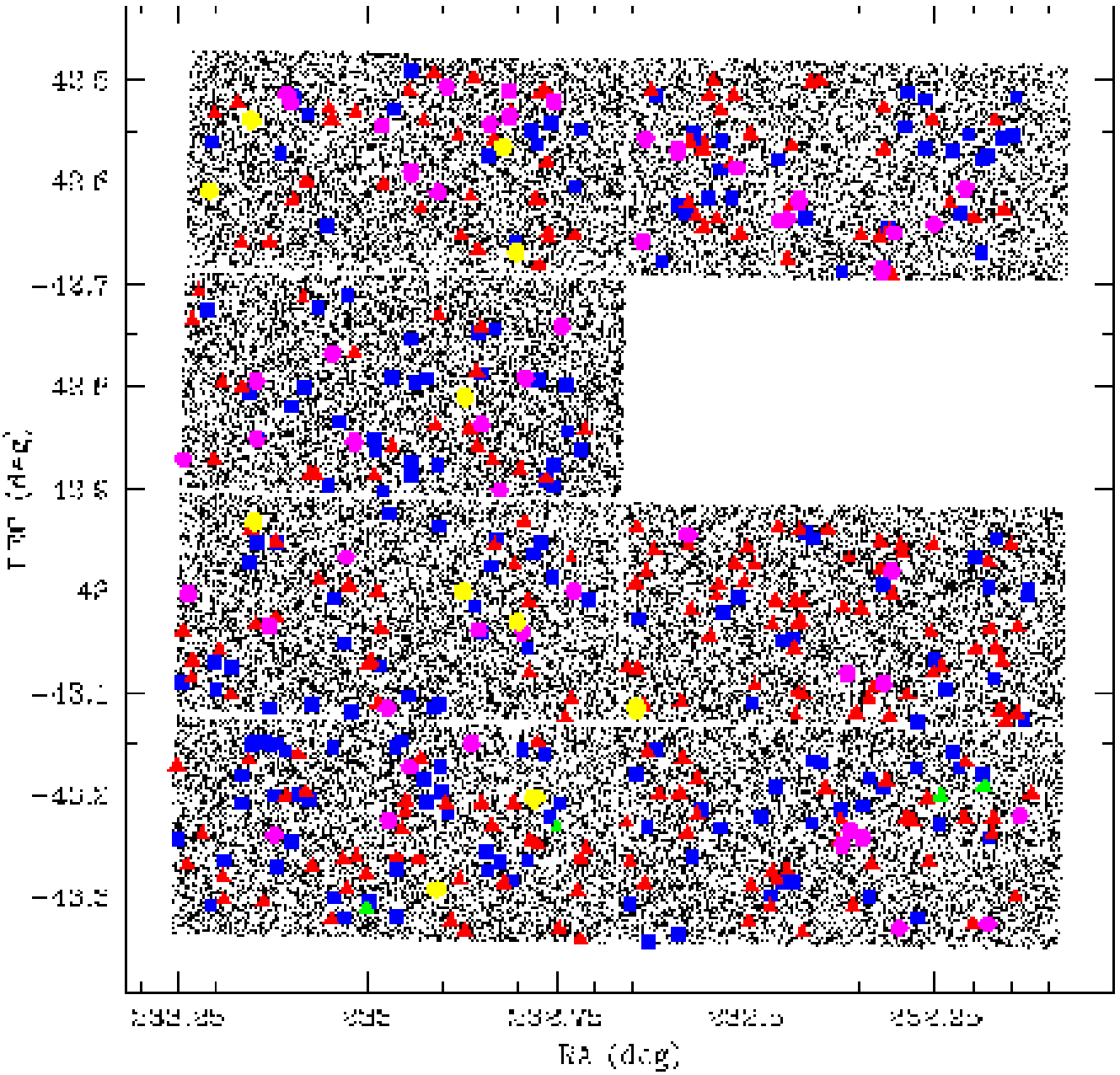

FIG. 3.— The astrometry for our field. The spatial distribution of the main types of variable are overplotted (with the same color schemes as in Fig. 2). The non-functional CCD7 is clear.

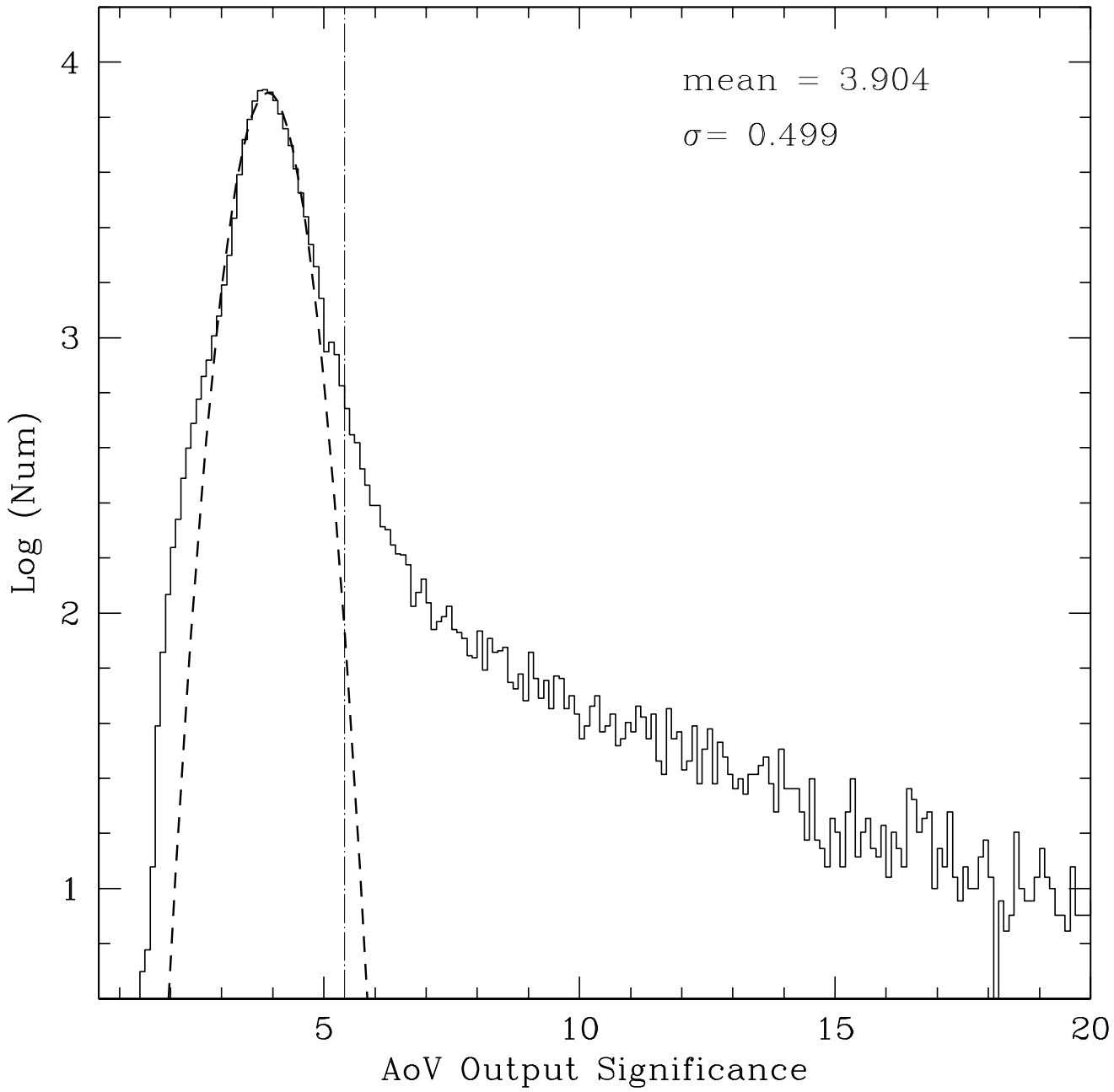

FIG. 4.— The output AoV significance (S_{AoV}) distribution for the whole 110,372 stellar lightcurve database upon which it was run. The main population at lower significance defines the general population for which no periodicity was detected. A Gaussian was fitted to this population and overplotted along with the resulting mean and standard deviation parameters. Any lightcurve that had an AoV output significance $\geq 3\times$ the standard deviation of the background (marked as a vertical line) was flagged as a candidate variable. All 9,230 candidates satisfying this criteria were searched for variability.

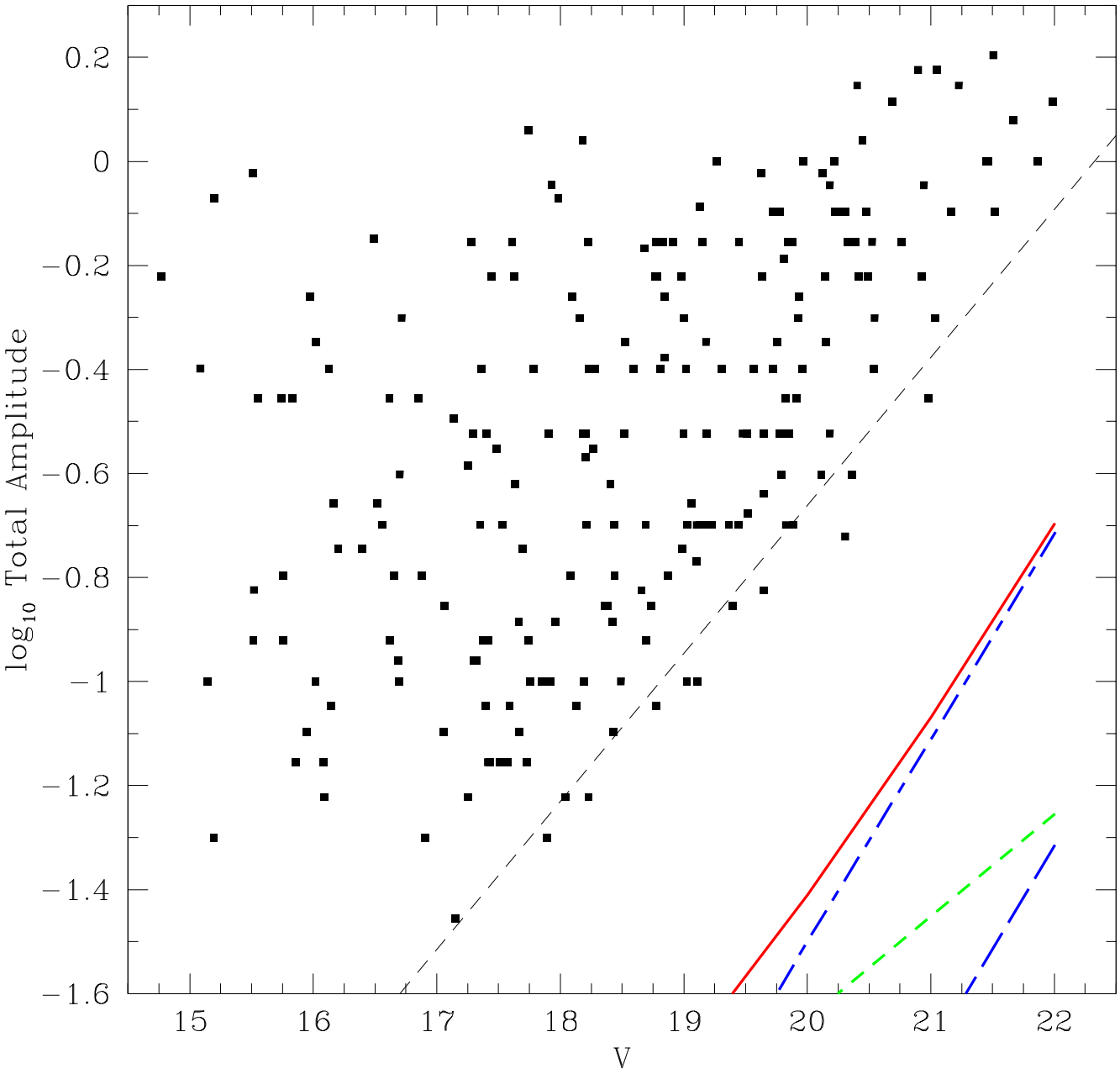

FIG. 5.— The total V+R amplitude for all variables presented in Figs. 8-17, plotted against their V magnitude. The empirical detection limit of our catalog is marked by the dotted line. Any variables with an amplitude below this line are unlikely to be detected in our survey. Also overplotted are the photometric noise contributions as per the color scheme of Fig. 1.

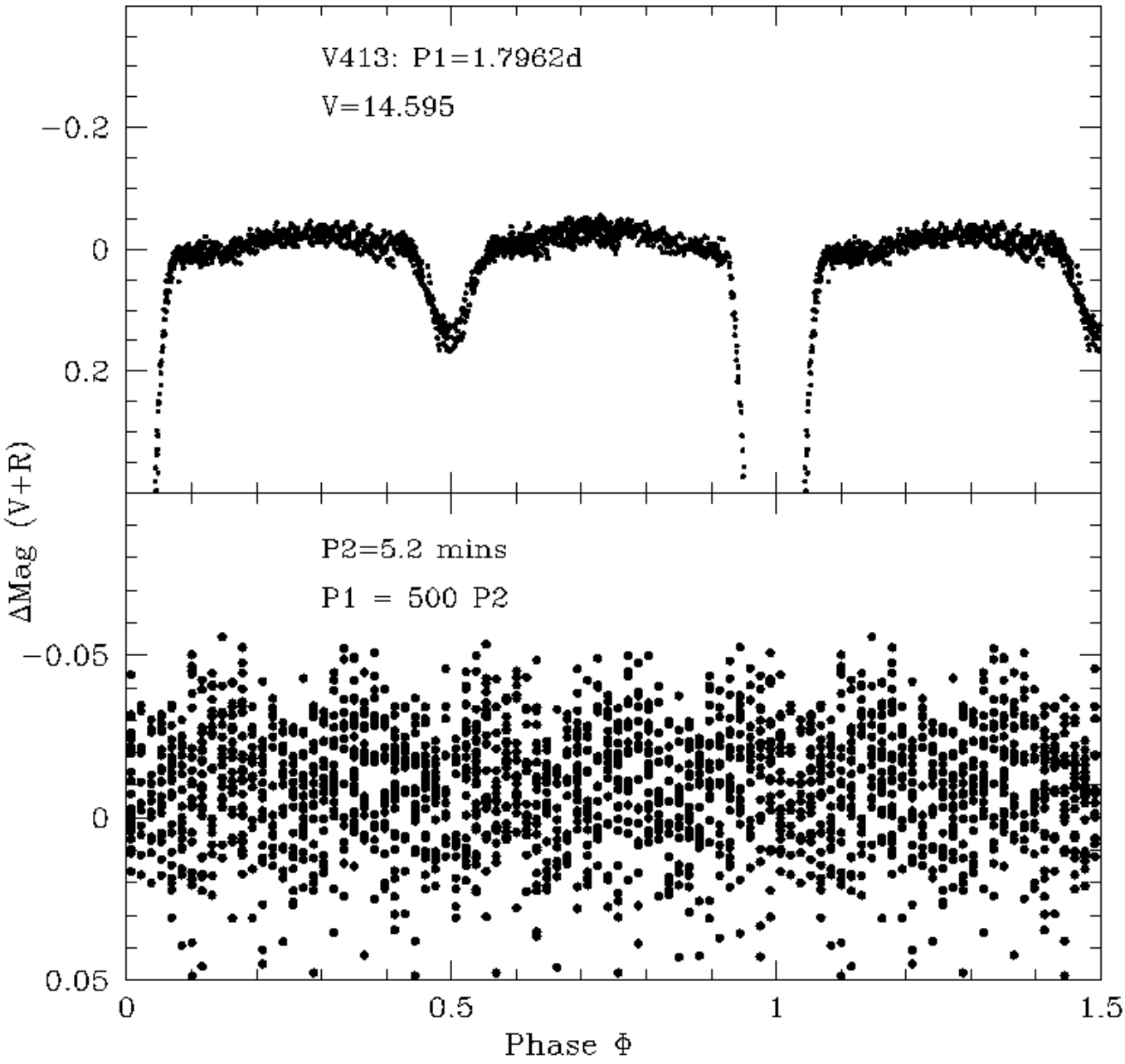

FIG. 6.— The small-scale pulsation variations of V413, as seen superimposed on the main binary lightcurve (top), and in close-up (bottom), phased wrapped to five times the 5.2 minute periodicity for ease of visibility. Such oscillations, present on the faint component of the binary, are perhaps induced by the companion, or indicative of a δ Scuti component.

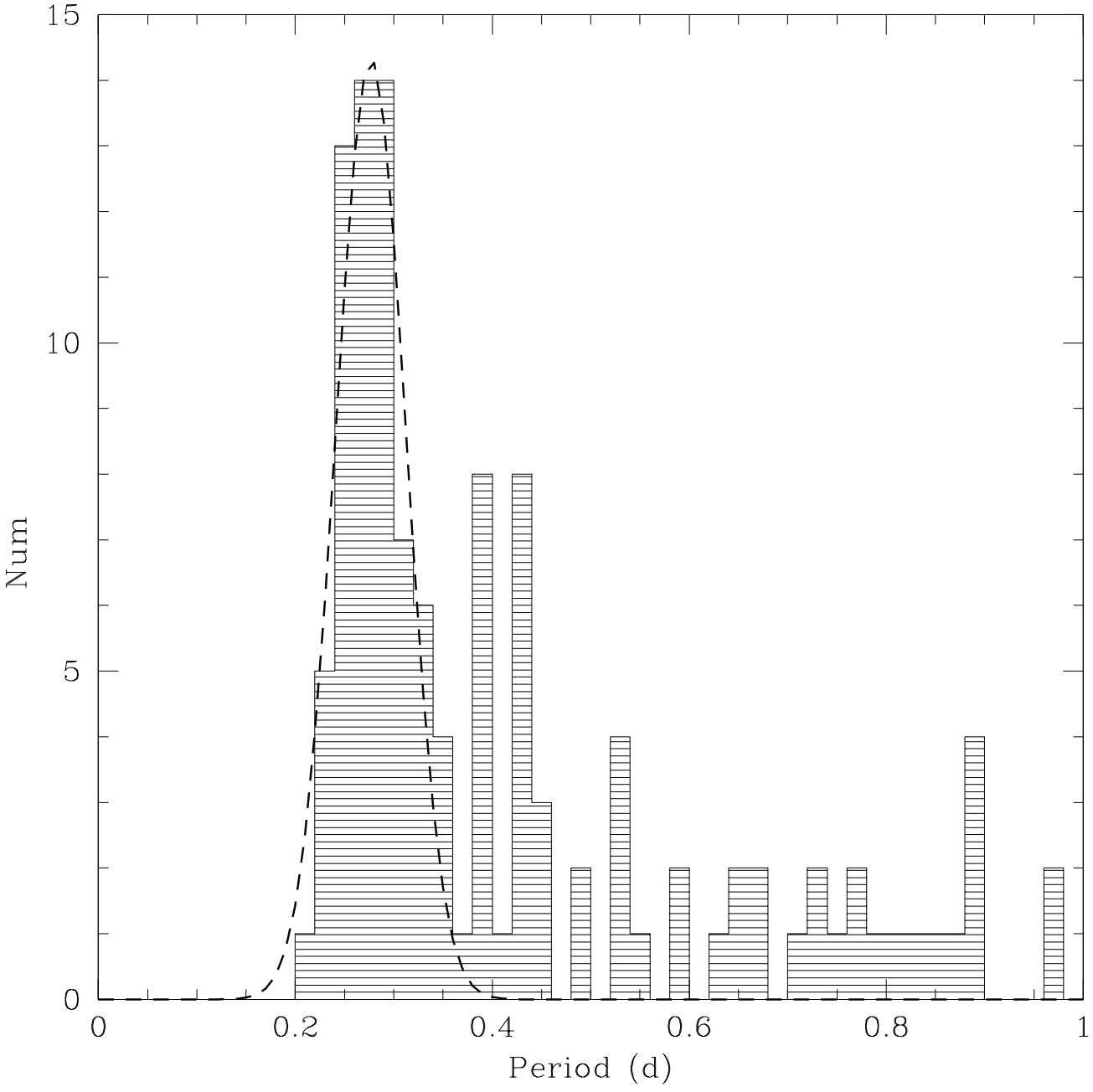

FIG. 7.— The $nP\ dP$ period distribution of all detected eclipsing binaries with period $\leq$1d. The shortest periods are well represented by a Gaussian with mean 0.277d and rms 0.036d. This population constitutes the W UMa stars. A decreasing tail to longer periods is also seen, which we attribute here to non W UMa contact and semi-detached binaries.

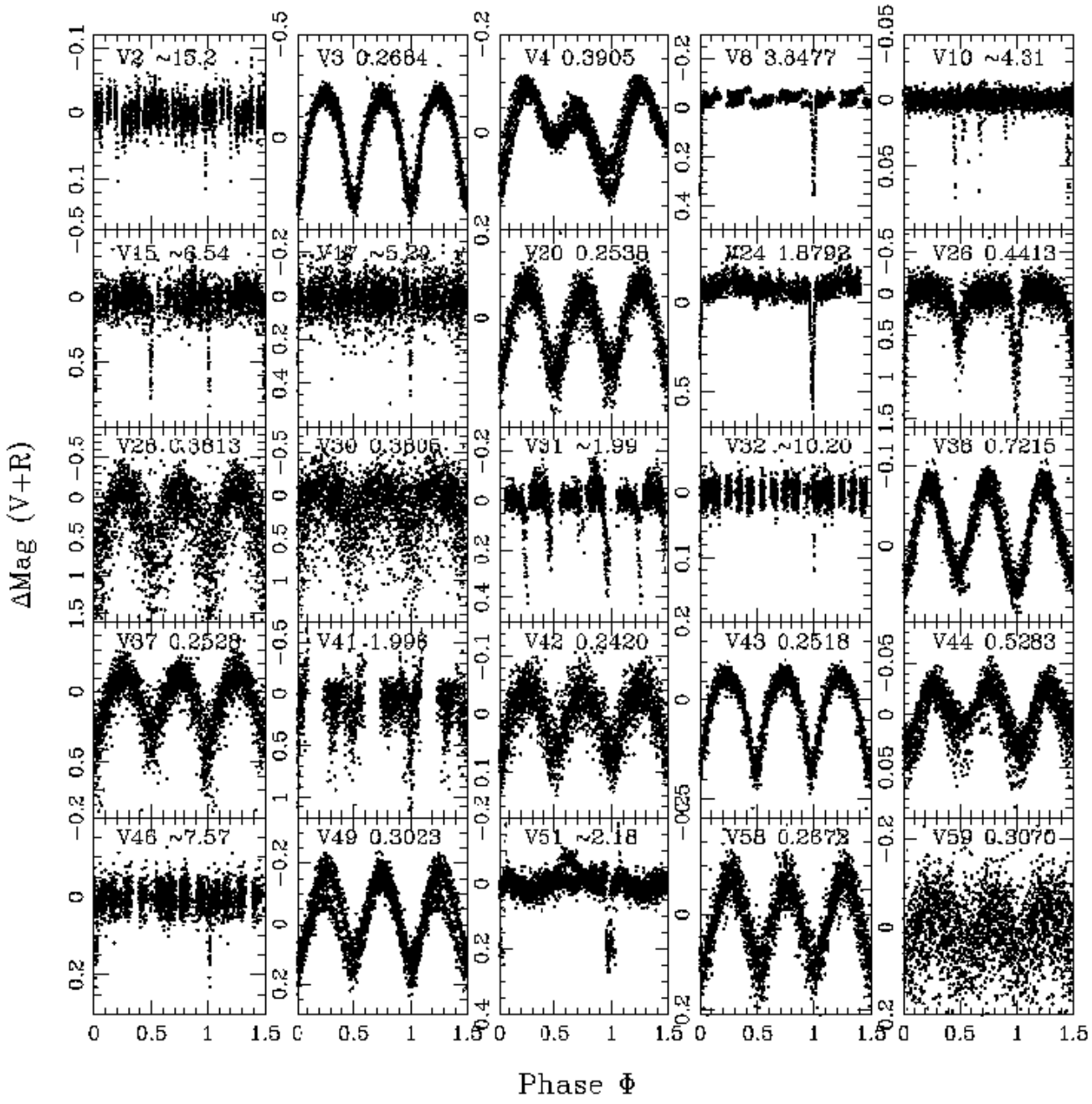

FIG. 8.— Phase-wrapped V+R lightcurves for the detected EcB. The identification and period (in days) are overplotted for each system.

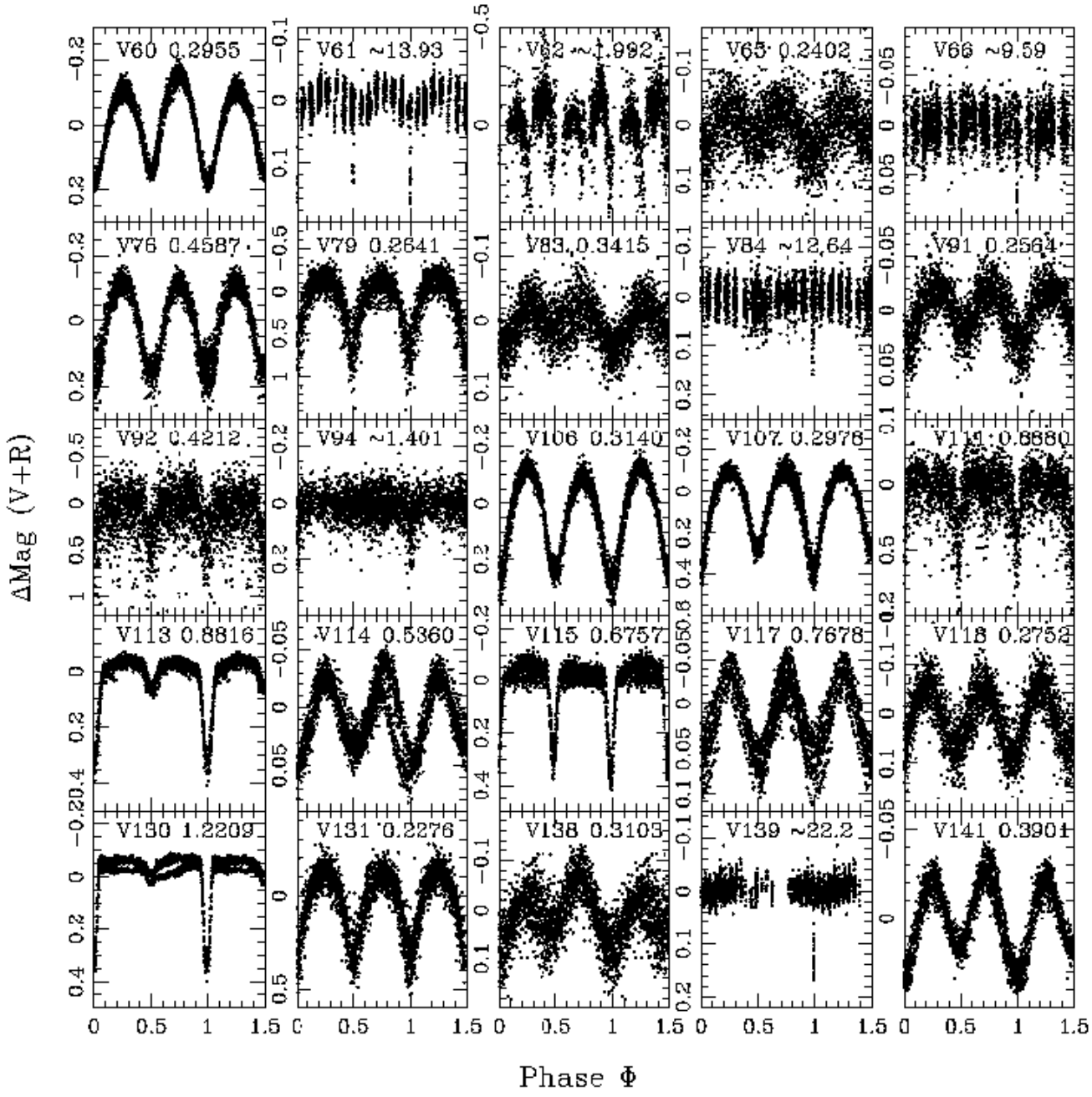

FIG. 9.— Binary lightcurves cont'd.

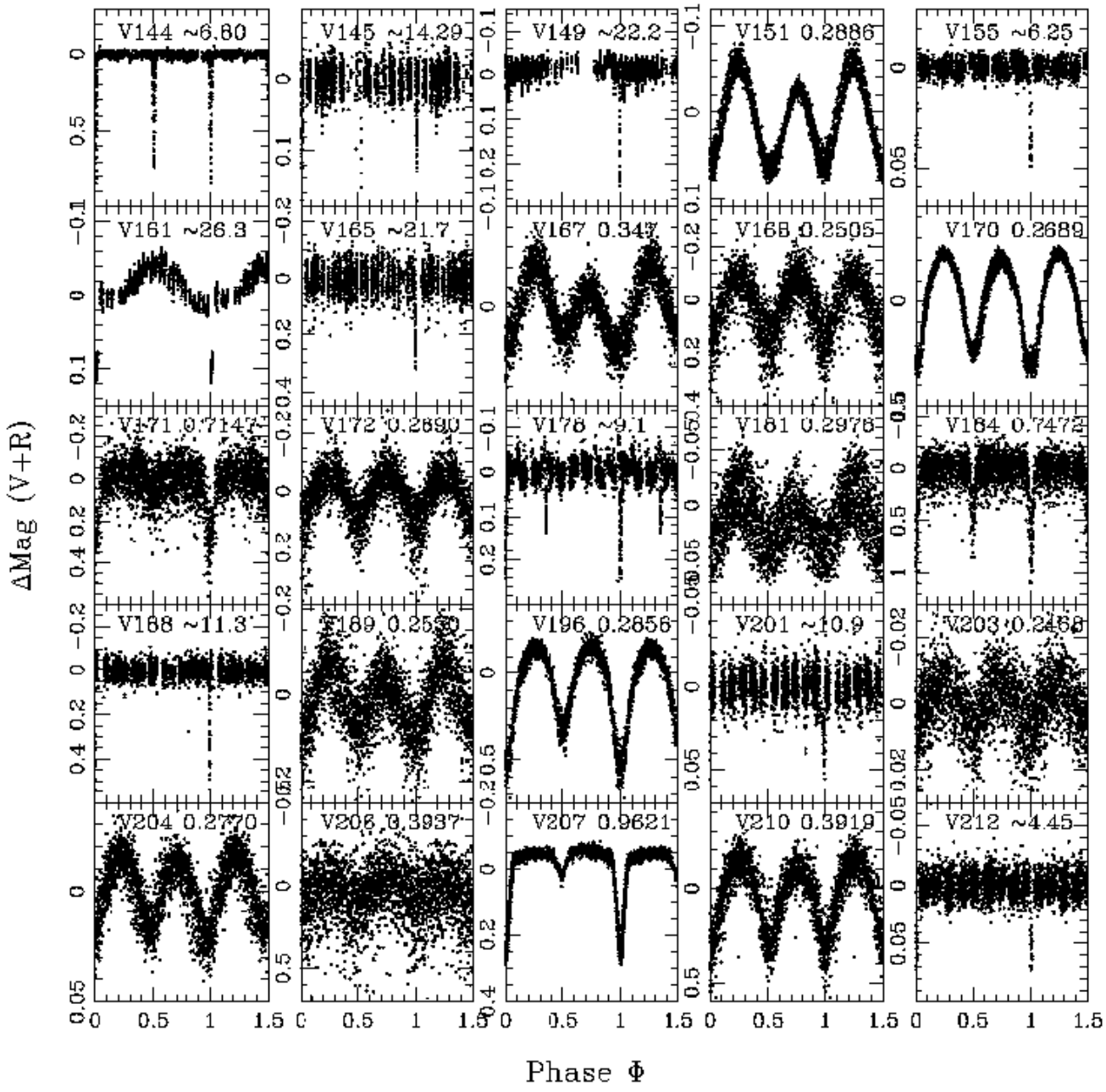

FIG. 10.— Binary lightcurves cont'd.

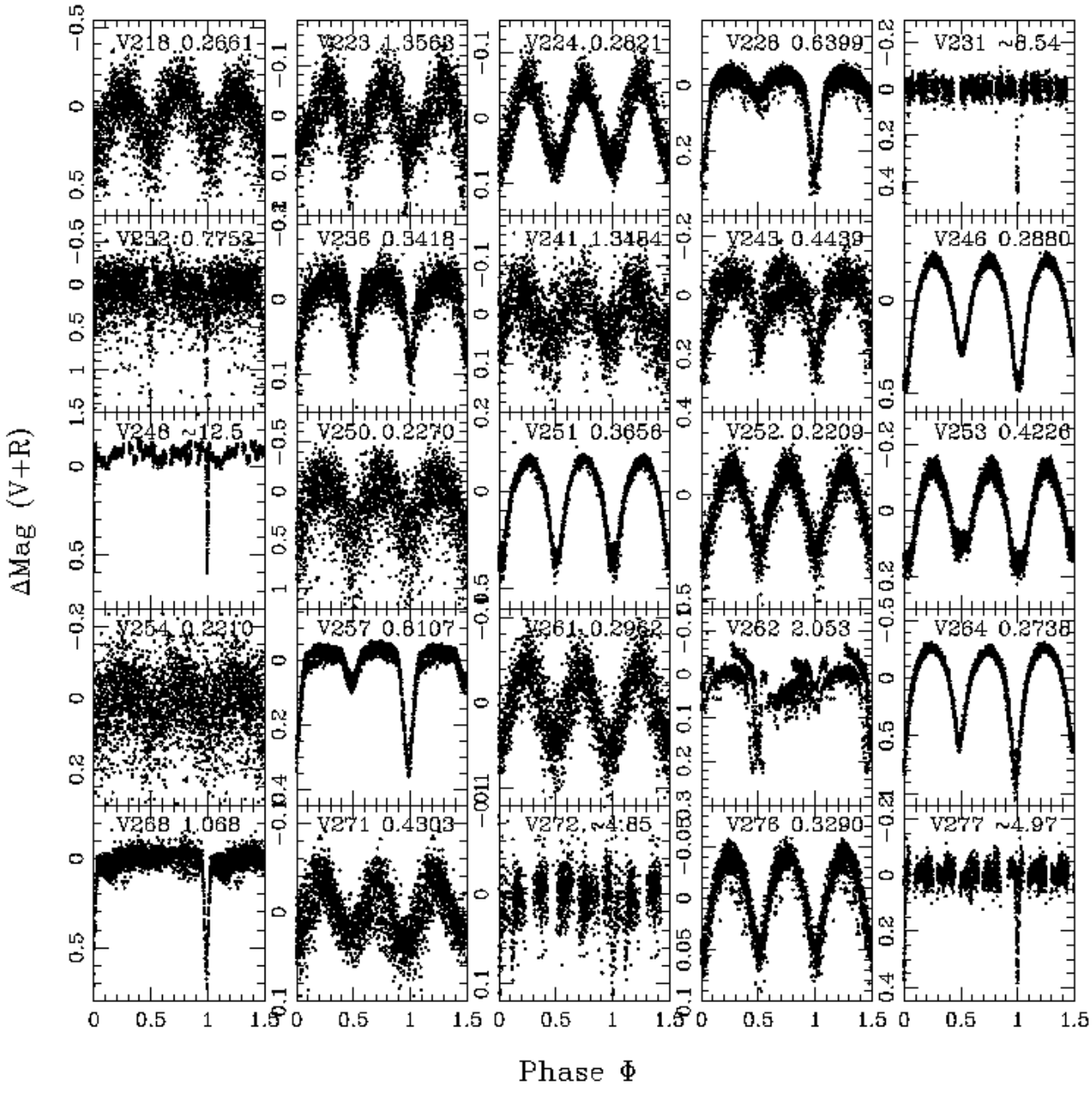

FIG. 11.— Binary lightcurves cont'd.

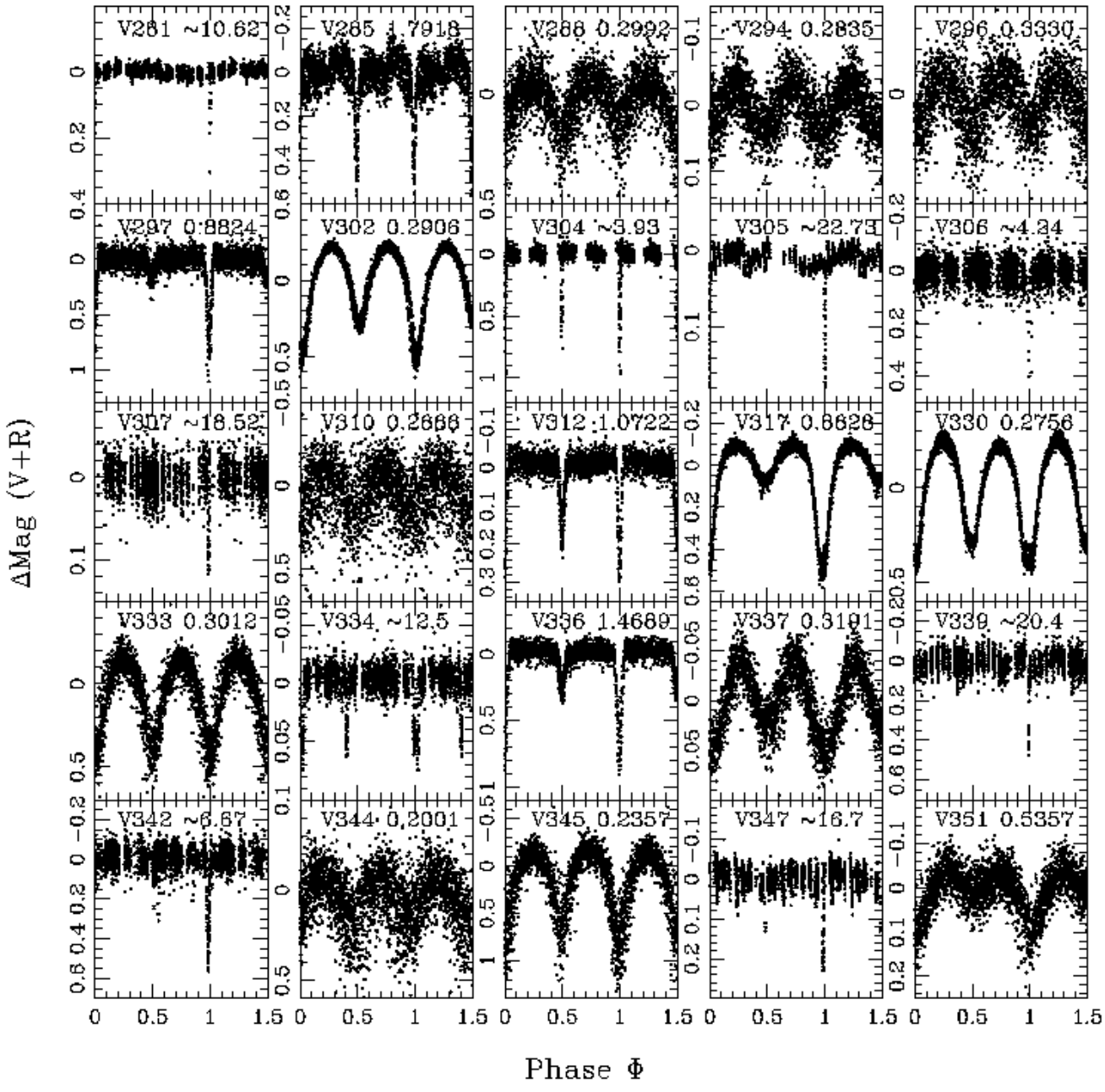

FIG. 12.— Binary lightcurves cont'd.

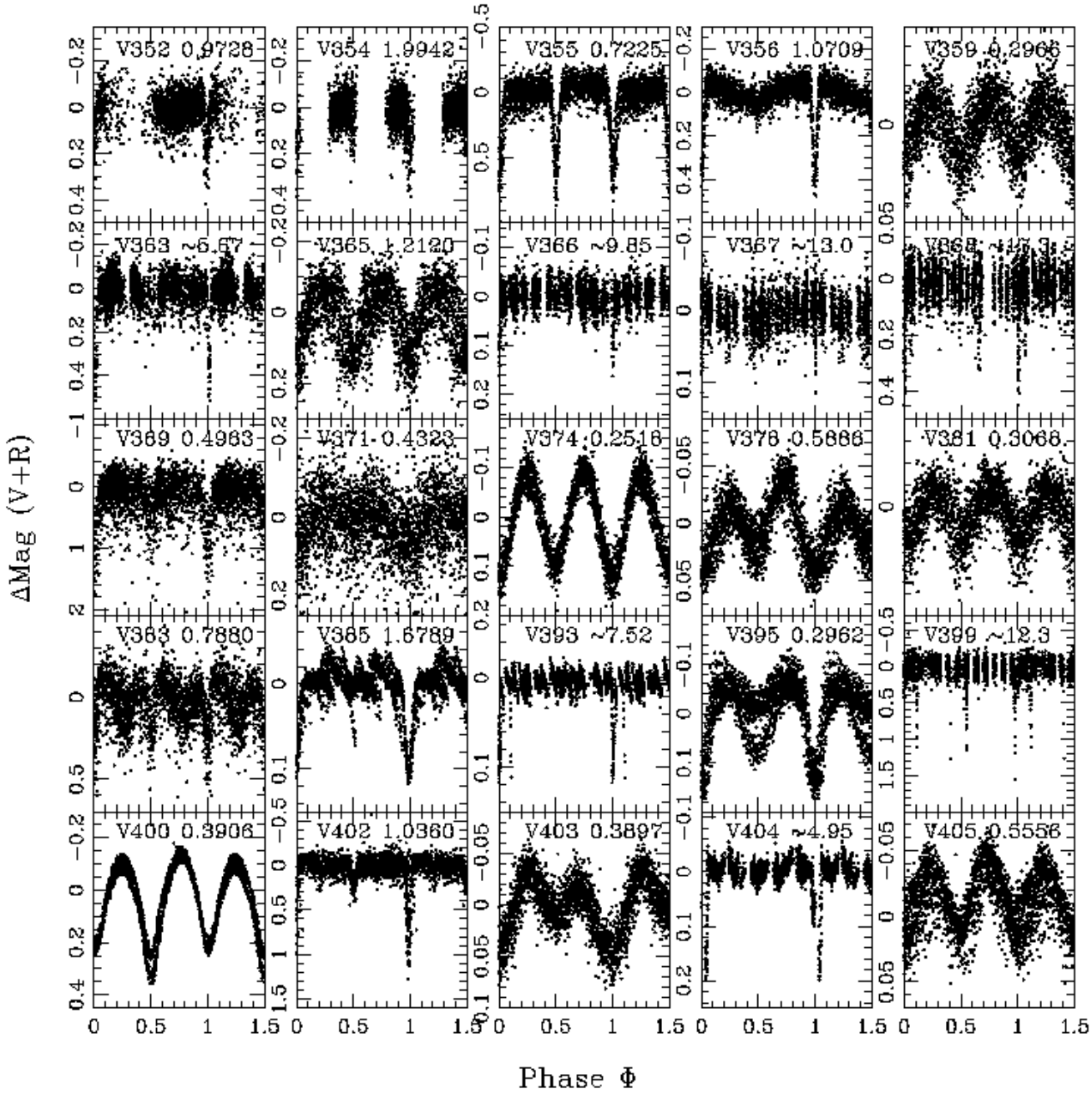

FIG. 13.— Binary lightcurves cont'd.

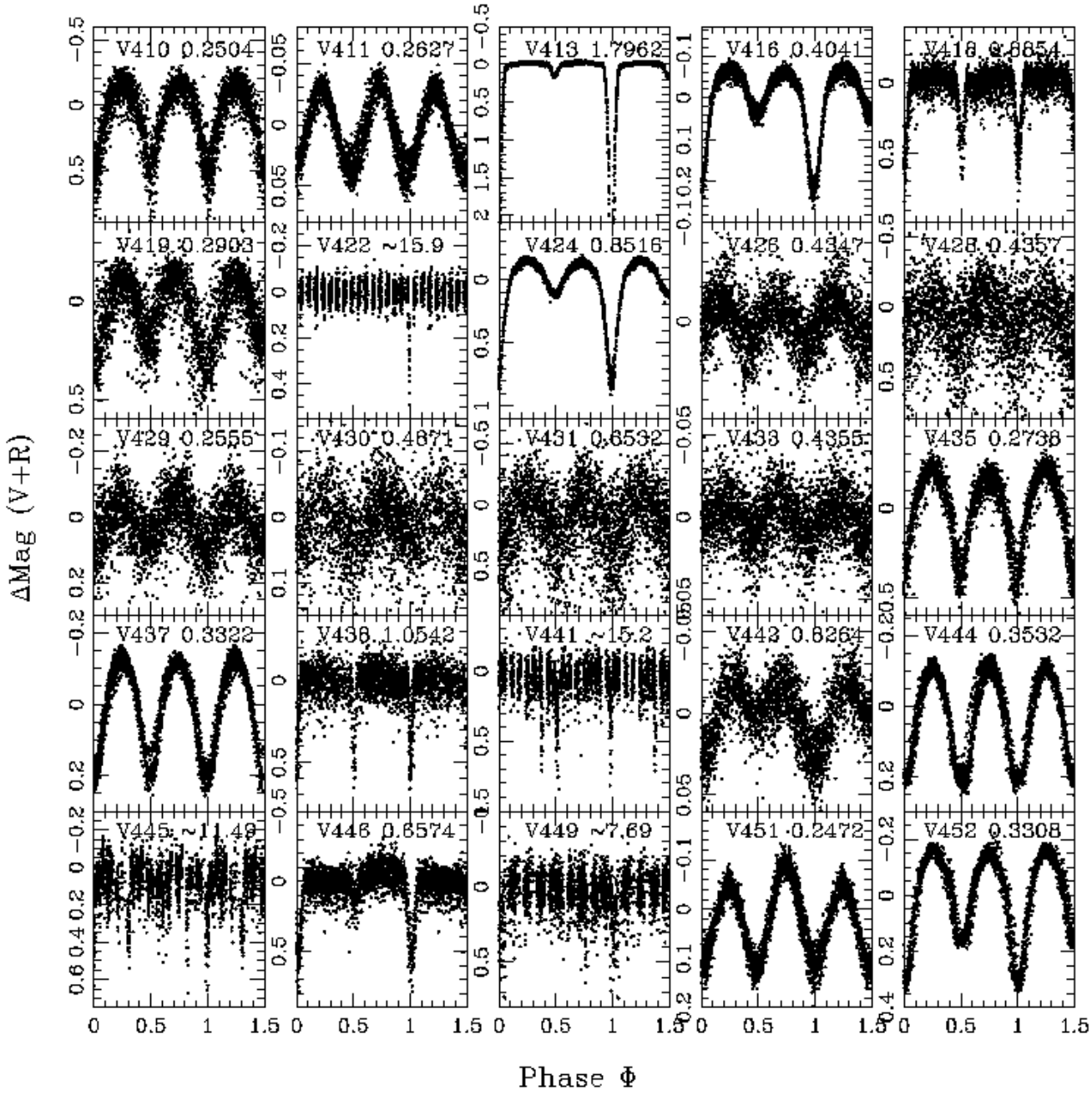

FIG. 14.— Binary lightcurves cont'd.

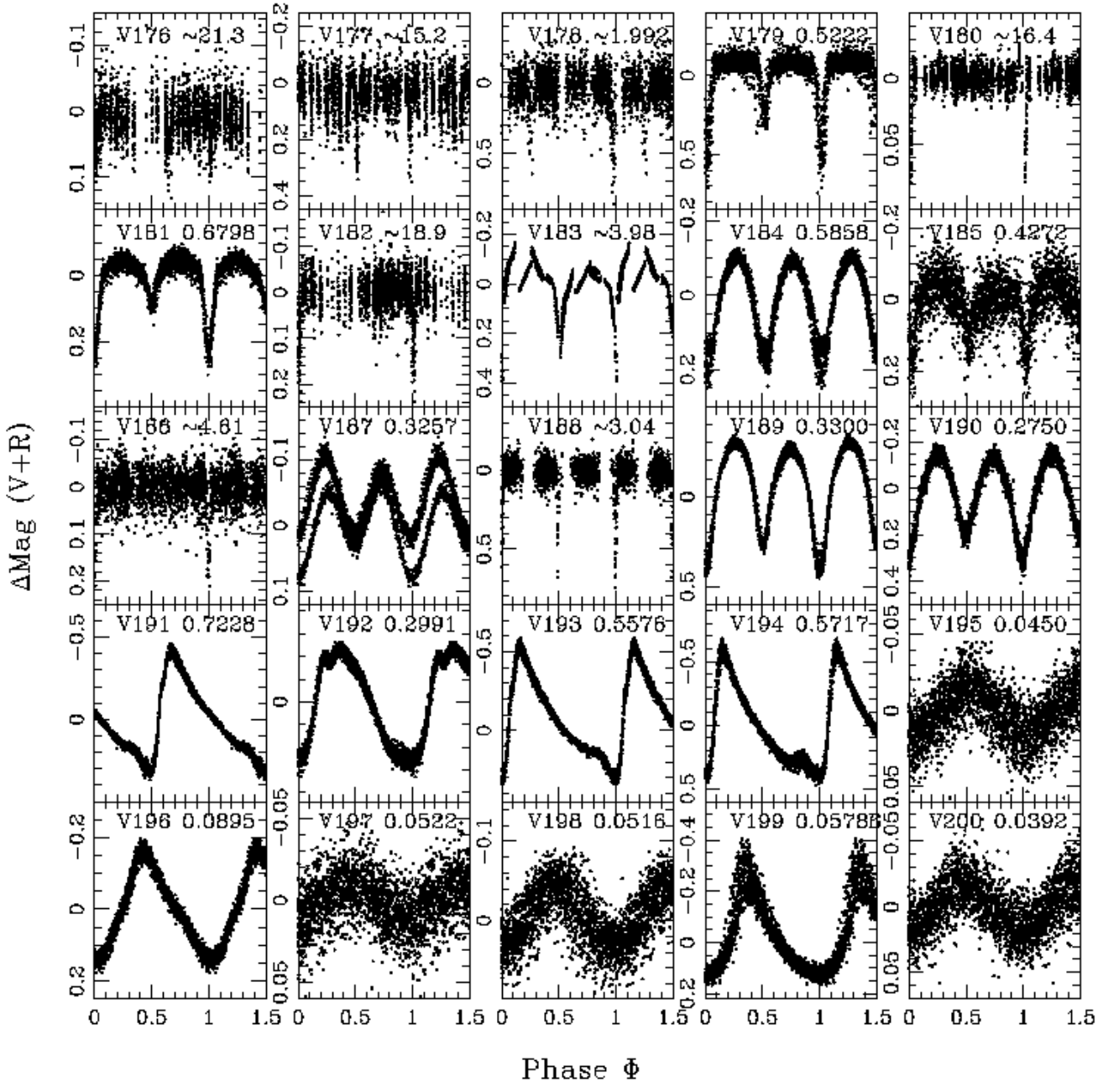

FIG. 15.— Binary, RR Lyrae (V191+) and δ Scuti (V195+) lightcurves.

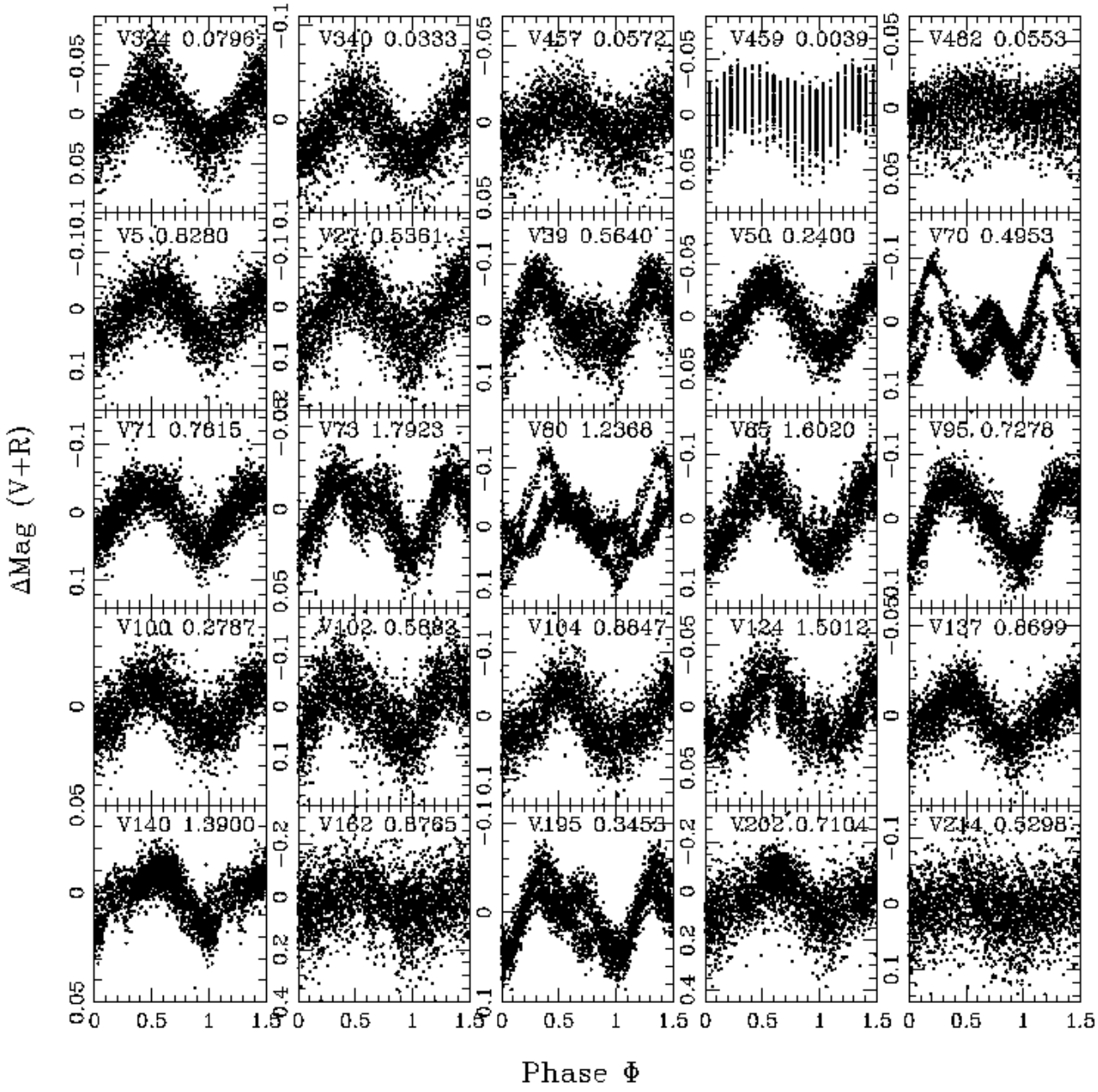

FIG. 16.— δ Scuti lightcurves cont'd and example pulsators (V5+).

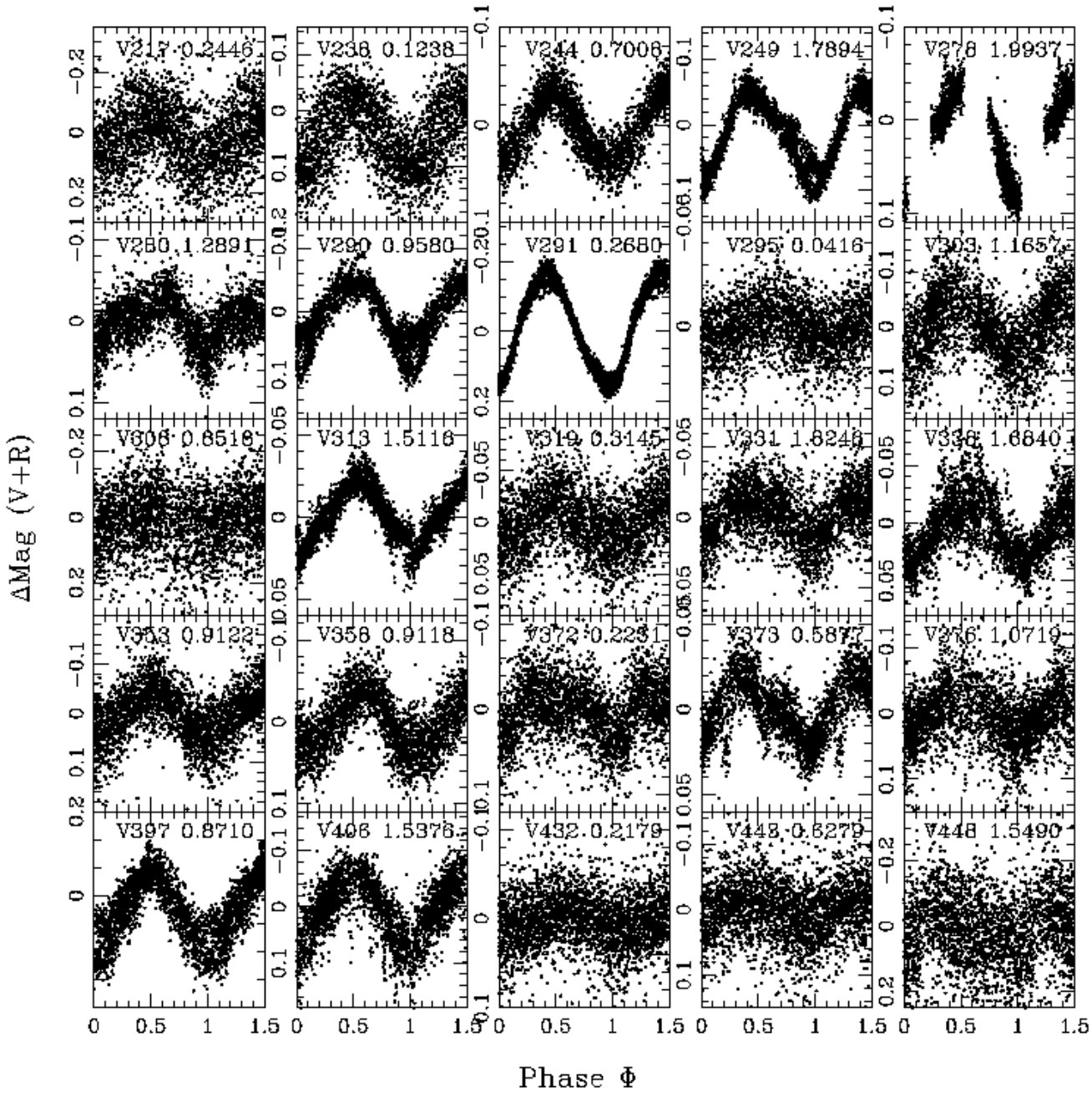

FIG. 17.— Example pulsators cont'd.

CCD	*RA(J2000.0)* h m s	*DEC(J2000.0)* ° ′ ″
1	15:31:47	−42:34:45
2	15:31:49	−42:47:35
3	15:31:50	−43:01:04
4	15:31:51	−43:13:57
5	15:29:30	−43:14:06
6	15:29:29	−43:01:07
7	–	–
8	15:29:27	−42:35:17

Table 1: Equatorial coordinates (J2000.0) for the centers of our CCDs. CCD7 was inoperative and is marked with a '−'.

ID	Type	Period (d)	RA (j2000.0) h m s	DEC (j2000.0) ° ′ ″	V	σV	V-I	σ(V-I)
V2	EcB	∼15.15	15:28:30.29	-42:59:51.98	18.187	0.005	0.744	0.008
V3	W UMa	0.26837	15:28:30.98	-43:00:17.23	18.830	0.006	0.779	0.008
V4	EcB	0.39051	15:28:31.49	-43:07:35.66	16.699	0.004	0.819	0.006
V8	EcB	3.84765	15:28:34.03	-42:31:00.60	15.739	0.005	0.838	0.013
V10	EcB	∼4.31	15:28:35.46	-42:33:17.75	15.860	0.003	0.660	0.007
V15	EcB	∼6.54	15:28:38.99	-42:33:23.34	20.309	0.017	0.945	0.022
V17	EcB	5.2915	15:28:40.56	-42:56:54.39	19.960	0.013	0.655	0.018
V20	W UMa	0.25374	15:28:41.36	-43:05:08.04	19.786	0.012	0.800	0.016
V24	EcB	1.87920	15:28:42.69	-42:59:47.78	18.982	0.007	1.224	0.009
V26	EcB	0.44130	15:28:43.13	-43:14:25.41	21.052	0.034	1.924	0.036
V28	W UMa	0.38132	15:28:43.58	-42:34:28.64	-	-	-	-
V30	W UMa	0.3805	15:28:44.60	-42:34:37.89	21.667	0.066	0.977	0.084
V31	EcB	∼1.99	15:28:44.78	-43:10:47.53	18.282	0.017	0.618	0.021
V32	EcB	∼10.20	15:28:45.73	-42:40:10.78	17.850	0.003	0.843	0.004
V36	EcB	0.72150	15:28:47.82	-42:58:03.82	16.657	0.002	0.414	0.003
V37	W UMa	0.25278	15:28:48.94	-42:33:14.88	20.181	0.022	0.960	0.026
V41	EcB	1.99634	15:28:51.92	-42:37:53.74	20.943	0.073	1.406	0.093
V42	W UMa	0.24198	15:28:52.59	-43:10:24.26	18.985	0.006	0.681	0.008
V43	W UMa	0.25179	15:28:53.83	-42:34:08.44	19.185	0.009	0.936	0.011
V44	EcB	0.5283	15:28:54.17	-43:09:26.08	15.145	0.004	0.342	0.016
V46	EcB	7.574	15:28:56.99	-43:05:43.42	20.307	0.014	0.670	0.023
V49	W UMa	0.30227	15:28:59.06	-43:13:37.12	18.844	0.006	0.962	0.008
V51	EcB	∼2.18	15:29:00.20	-43:03:58.98	18.437	0.005	1.068	0.007
V58	W UMa	0.26719	15:29:03.34	-42:33:53.89	19.000	0.008	0.843	0.011
V59	W UMa	0.30699	15:29:03.53	-42:31:08.95	19.885	0.012	0.682	0.017
V60	W UMa	0.29546	15:29:05.20	-43:07:41.87	15.832	0.004	0.807	0.012
V61	EcB	13.926	15:29:05.65	-43:19:09.02	16.881	0.012	0.853	0.014
V62	EcB	∼1.99	15:29:06.26	-43:10:21.02	-	-	-	-
V65	W UMa	0.24015	15:29:08.87	-42:30:45.17	19.363	0.007	1.162	0.009
V66	EcB	∼9.59	15:29:09.23	-42:32:49.89	18.779	0.007	2.204	0.008
V76	EcB	0.45872	15:29:14.77	-42:38:36.87	18.226	0.008	0.454	0.013
V79	W UMa	0.26406	15:29:15.99	-42:40:58.84	20.690	0.034	1.001	0.040
V83	W UMa	0.34154	15:29:16.59	-43:11:37.26	19.397	0.009	2.151	0.010
V84	EcB	12.64	15:29:16.61	-42:59:34.17	18.876	0.006	0.688	0.008
V91	W UMa	0.2564	15:29:20.71	-43:10:56.27	18.132	0.004	0.918	0.006
V92	EcB	0.42122	15:29:20.84	-43:17:55.92	21.863	0.066	1.353	0.079
V94	EcB	∼1.40	15:29:23.10	-43:12:35.69	19.826	0.014	0.912	0.019
V106	W UMa	0.31400	15:29:30.08	-42:41:12.99	18.162	0.005	0.712	0.007
V107	W UMa	0.29784	15:29:30.34	-43:12:50.70	18.788	0.014	0.815	0.018
V111	EcB	0.88795	15:29:36.30	-43:10:03.20	21.168	0.047	1.326	0.050
V113	EcB	0.88159	15:29:38.56	-42:56:55.11	16.024	0.002	0.346	0.005
V114	EcB	0.5360	15:29:39.23	-43:09:59.61	16.688	0.003	0.730	0.005
V115	EcB	0.67566	15:29:39.31	-43:13:31.04	18.595	0.006	0.860	0.007
V117	EcB	0.76777	15:29:40.83	-42:38:03.16	15.519	0.003	0.480	0.005
V118	W UMa	0.27518	15:29:41.11	-42:56:30.49	19.029	0.013	0.848	0.016
V130	EcB	1.22086	15:29:44.70	-43:02:48.30	16.128	0.002	0.718	0.005
V131	W UMa	0.22763	15:29:44.70	-43:17:03.90	19.843	0.022	1.026	0.029
V138	W UMa	0.3103	15:29:48.59	-43:02:52.47	19.061	0.013	0.701	0.022

ID	Type	Period (d)	RA (j2000.0) h m s	DEC (j2000.0) ° ′ ″	V	σV	V-I	σ(V-I)
V139	EcB	∼22.22	15:29:48.82	-43:16:58.56	17.694	0.004	0.686	0.006
V141	EcB	0.39008	15:29:49.42	-42:34:39.26	15.947	0.002	0.773	0.004
V144	EcB	6.8016	15:29:50.27	-43:11:33.10	17.931	0.008	0.871	0.011
V145	EcB	∼14.29	15:29:50.34	-43:11:31.14	18.442	0.019	1.129	0.022
V149	EcB	∼22.22	15:29:52.08	-43:17:48.50	17.251	0.003	0.672	0.006
V151	W UMa	0.28859	15:29:55.18	-43:13:13.61	15.754	0.007	0.680	0.018
V155	EcB	6.2499	15:29:58.17	-43:06:31.31	15.195	0.002	-	-
V161	EcB	∼26.29	15:30:02.45	-43:00:18.92	16.394	0.003	0.955	0.009
V165	EcB	∼21.74	15:30:04.23	-42:37:00.12	19.509	0.011	0.664	0.015
V167	W UMa	0.347	15:30:07.20	-43:01:11.10	17.746	0.005	0.776	0.010
V168	W UMa	0.25049	15:30:07.91	-42:33:38.39	19.756	0.010	0.402	0.020
V170	W UMa	0.26889	15:30:08.27	-42:35:09.22	18.097	0.004	0.879	0.005
V171	EcB	0.71467	15:30:08.27	-43:13:53.74	20.152	0.024	0.560	0.039
V172	W UMa	0.26898	15:30:08.48	-42:35:11.50	19.649	0.016	1.061	0.018
V178	EcB	9.111	15:30:11.46	-42:36:57.65	18.406	0.005	0.945	0.006
V181	W UMa	0.29761	15:30:13.45	-42:33:41.15	17.322	0.003	1.226	0.004
V184	EcB	0.74719	15:30:14.41	-43:12:45.97	21.448	0.047	2.602	0.048
V188	EcB	∼11.30	15:30:16.82	-42:33:04.76	18.844	0.007	0.692	0.009
V189	W UMa	0.25502	15:30:17.21	-43:15:34.25	19.824	0.011	0.961	0.014
V196	W UMa	0.28558	15:30:18.40	-42:37:55.20	19.129	0.008	0.963	0.011
V201	EcB	∼10.87	15:30:20.94	-43:20:07.91	16.907	0.007	0.613	0.012
V203	W UMa	0.24680	15:30:21.55	-42:37:22.49	17.151	0.004	0.721	0.009
V204	W UMa	0.27700	15:30:26.72	-42:40:42.60	16.519	0.004	0.989	0.007
V206	EcB	0.39372	15:30:28.20	-42:30:53.15	21.036	0.038	1.075	0.046
V207	EcB	0.96208	15:30:28.37	-43:09:15.62	16.850	0.016	0.658	0.020
V210	EcB	0.39185	15:30:30.62	-43:20:34.62	19.809	0.015	0.919	0.018
V212	EcB	∼4.45	15:30:31.41	-43:13:50.00	17.515	0.005	0.670	0.007
V218	W UMa	0.26605	15:30:33.91	-43:01:35.66	20.762	0.031	0.728	0.043
V223	EcB	1.35629	15:30:34.85	-43:10:43.63	19.521	0.012	1.322	0.014
V224	W UMa	0.28208	15:30:36.66	-43:18:22.33	17.349	0.005	1.172	0.006
V228	EcB	0.63984	15:30:49.60	-43:00:30.86	15.553	0.003	0.455	0.005
V231	EcB	8.5470	15:30:52.24	-42:51:39.28	18.527	0.009	0.784	0.013
V232	EcB	0.77521	15:30:52.28	-42:32:53.14	21.985	0.066	2.910	0.067
V236	W UMa	0.34175	15:30:53.68	-42:36:16.14	18.361	0.004	2.028	0.006
V241	EcB	1.3484	15:30:56.15	-42:50:40.36	19.227	0.010	1.343	0.012
V243	EcB	0.44388	15:30:57.35	-42:47:51.39	19.304	0.013	1.502	0.014
V246	W UMa	0.28803	15:30:59.40	-43:12:28.72	17.280	0.003	0.777	0.005
V248	EcB	∼12.50	15:31:00.46	-42:53:46.96	17.612	0.007	1.060	0.009
V250	W UMa	0.22700	15:31:01.31	-42:52:32.17	21.226	0.053	0.820	0.070
V251	W UMa	0.36560	15:31:01.84	-42:59:14.87	17.627	0.025	0.635	0.037
V252	W UMa	0.22092	15:31:01.99	-42:32:30.18	19.632	0.012	1.138	0.016
V253	EcB	0.42261	15:31:02.16	-43:13:15.08	17.906	0.003	0.370	0.006
V254	W UMa	0.22100	15:31:02.24	-42:32:31.10	20.362	0.020	1.378	0.026
V257	EcB	0.81069	15:31:02.97	-42:53:23.87	15.086	0.007	0.437	0.011
V261	W UMa	0.29620	15:31:04.04	-43:09:36.05	18.871	0.005	0.680	0.007
V262	EcB	∼2.05	15:31:04.77	-42:57:10.27	16.163	0.010	0.629	0.016
V264	W UMa	0.27379	15:31:05.24	-42:47:35.15	17.664	0.007	1.136	0.009
V268	EcB	1.06799	15:31:06.41	-42:33:47.29	18.914	0.006	1.187	0.008
V271	EcB	0.43028	15:31:07.11	-42:57:47.33	18.379	0.008	0.989	0.011

ID	Type	Period (d)	RA (j2000.0) h m s	DEC (j2000.0) ° ′ ″	V	σV	V-I	σ(V-I)
V272	EcB	4.85015	15:31:07.73	-42:32:57.29	17.920	0.014	0.665	0.018
V276	W UMa	0.32895	15:31:09.15	-43:03:25.33	15.755	0.007	0.679	0.025
V277	EcB	∼4.97	15:31:09.15	-43:15:48.63	18.812	0.006	0.713	0.009
V281	EcB	∼10.62	15:31:11.04	-43:09:16.77	17.403	0.020	0.743	0.030
V285	EcB	1.79179	15:31:13.33	-42:39:28.98	18.778	0.011	0.640	0.016
V288	W UMa	0.29922	15:31:13.99	-43:16:54.92	20.493	0.026	0.710	0.047
V294	W UMa	0.28345	15:31:18.01	-43:15:55.56	18.989	0.012	0.463	0.015
V296	W UMa	0.33300	15:31:18.78	-42:56:52.86	20.567	0.023	0.384	0.034
V297	EcB	0.88242	15:31:19.61	-42:44:36.06	19.967	0.019	1.560	0.021
V302	W UMa	0.29058	15:31:20.66	-42:58:33.50	17.987	0.004	0.916	0.006
V304	EcB	3.9356	15:31:21.14	-42:34:28.85	19.264	0.008	2.397	0.009
V305	EcB	∼22.73	15:31:21.81	-43:16:22.69	16.200	0.002	0.690	0.005
V306	EcB	∼4.24	15:31:22.09	-43:15:13.20	19.720	0.010	0.886	0.013
V307	EcB	∼18.52	15:31:23.22	-43:02:24.95	18.695	0.004	0.618	0.008
V310	W UMa	0.26656	15:31:23.77	-42:47:17.32	20.415	0.028	0.838	0.036
V312	EcB	1.07219	15:31:24.33	-42:44:50.66	18.209	0.008	1.241	0.011
V317	EcB	0.86278	15:31:25.92	-43:00:49.14	18.680	0.006	0.439	0.009
V330	W UMa	0.27555	15:31:34.44	-43:12:59.60	18.229	0.004	0.817	0.007
V333	W UMa	0.30121	15:31:36.09	-43:11:45.10	19.721	0.016	0.650	0.021
V334	EcB	∼12.50	15:31:37.13	-43:10:16.74	17.575	0.003	0.662	0.005
V336	EcB	1.46889	15:31:37.47	-42:56:07.74	19.629	0.009	0.754	0.011
V337	W UMa	0.3191	15:31:37.48	-43:06:45.02	18.421	0.005	0.768	0.008
V339	EcB	∼20.41	15:31:37.79	-42:52:30.58	19.003	0.052	0.887	0.081
V342	EcB	6.6675	15:31:38.49	-43:06:52.80	19.933	0.014	0.583	0.019
V344	W UMa	0.2009	15:31:41.31	-43:12:17.09	20.925	0.027	1.014	0.034
V345	W UMa	0.23572	15:31:41.36	-42:47:33.09	20.404	0.036	1.321	0.039
V347	EcB	∼16.67	15:31:42.08	-43:11:04.15	18.514	0.006	0.722	0.008
V351	EcB	0.53566	15:31:44.85	-42:47:44.64	18.264	0.009	0.794	0.014
V352	EcB	0.97276	15:31:45.72	-42:53:13.03	19.853	0.021	1.855	0.022
V354	EcB	1.99421	15:31:45.98	-42:29:26.55	19.478	0.012	1.088	0.019
V355	EcB	0.7225	15:31:46.46	-42:45:05.96	20.126	0.019	1.605	0.023
V356	EcB	1.07088	15:31:46.49	-42:52:23.93	19.180	0.012	1.392	0.014
V359	W UMa	0.29655	15:31:46.85	-43:06:06.24	18.226	0.010	1.388	0.012
V363	EcB	∼5.67	15:31:49.28	-43:08:41.05	19.923	0.011	0.675	0.015
V365	EcB	1.21198	15:31:50.64	-43:19:08.61	19.804	0.013	1.530	0.015
V366	EcB	∼9.85	15:31:50.90	-43:16:17.33	18.657	0.011	0.619	0.014
V367	EcB	∼12.99	15:31:51.29	-43:09:04.00	19.024	0.006	1.307	0.007
V368	EcB	∼17.25	15:31:51.56	-42:31:39.91	19.568	0.007	0.694	0.015
V369	EcB	0.49627	15:31:52.01	-42:47:27.83	21.507	0.056	1.279	0.068
V371	EcB	0.43234	15:31:52.65	-42:55:30.38	20.113	0.017	1.434	0.018
V374	W UMa	0.25177	15:31:54.55	-42:54:06.47	18.183	0.006	1.200	0.012
V378	EcB	0.58859	15:31:55.98	-43:04:22.07	17.753	0.004	0.930	0.006
V381	W UMa	0.30676	15:31:56.81	-42:51:41.51	19.804	0.014	0.559	0.022
V383	EcB	0.78798	15:31:57.82	-42:51:06.44	20.390	0.024	1.129	0.028
V385	EcB	1.67889	15:31:59.34	-43:18:09.60	15.514	0.003	0.244	0.006
V393	EcB	∼7.52	15:32:05.09	-43:07:08.12	16.622	0.004	0.676	0.007
V395	W UMa	0.29619	15:32:05.78	-42:42:36.44	17.483	0.004	1.365	0.007
V399	EcB	∼12.35	15:32:06.93	-43:03:03.05	20.896	0.025	1.219	0.035
V400	EcB	0.39061	15:32:06.95	-43:19:09.01	16.715	0.006	0.641	0.010

ID	Type	Period (d)	RA (j2000.0) h m s	DEC (j2000.0) ° ′ ″	V	σV	V-I	σ(V-I)
V402	EcB	1.03601	15:32:08.91	-42:49:59.62	20.448	0.025	2.078	0.027
V403	EcB	0.3897	15:32:10.49	-43:00:22.49	17.957	0.008	0.781	0.009
V404	EcB	∼4.95	15:32:10.70	-43:18:01.36	17.529	0.003	0.685	0.004
V405	EcB	0.55556	15:32:10.87	-43:09:09.48	16.694	0.002	0.272	0.005
V410	W UMa	0.25039	15:32:12.42	-42:53:43.14	20.217	0.022	1.242	0.025
V411	W UMa	0.26266	15:32:12.96	-42:38:31.50	16.143	0.003	0.748	0.004
V413	EcB	1.7962	15:32:15.56	-42:43:21.56	14.595	0.008	-	-
V416	EcB	0.40409	15:32:17.81	-43:06:37.05	17.136	0.005	0.513	0.008
V418	EcB	0.88544	15:32:18.21	-43:12:10.65	20.479	0.022	1.337	0.025
V419	W UMa	0.29027	15:32:18.32	-42:32:01.71	19.874	0.050	0.971	0.051
V422	EcB	15.8725	15:32:20.04	-42:48:03.65	19.016	0.011	0.852	0.013
V424	EcB	0.85157	15:32:20.95	-43:11:56.56	18.178	0.004	0.554	0.006
V426	EcB	0.43466	15:32:22.80	-42:31:04.24	18.432	0.006	0.861	0.009
V428	EcB	0.43572	15:32:23.27	-42:31:16.79	21.520	0.048	1.806	0.055
V429	W UMa	0.2555	15:32:23.43	-43:14:42.79	20.181	0.022	0.841	0.030
V430	EcB	0.48709	15:32:23.66	-42:49:05.10	19.107	0.012	0.630	0.016
V431	EcB	0.65315	15:32:23.77	-42:30:51.84	21.469	0.057	0.823	0.073
V433	EcB	0.43546	15:32:24.83	-42:31:09.56	17.888	0.003	0.591	0.005
V435	W UMa	0.27377	15:32:25.52	-43:09:23.93	19.778	0.010	0.818	0.013
V437	W UMa	0.33218	15:32:27.21	-42:34:14.80	17.783	0.003	0.662	0.006
V438	EcB	1.05423	15:32:28.48	-43:16:09.16	20.326	0.040	1.876	0.044
V441	EcB	∼15.15	15:32:28.89	-43:08:58.22	20.242	0.019	0.810	0.022
V442	EcB	0.8264	15:32:28.90	-42:57:08.37	17.588	0.006	0.498	0.009
V444	W UMa	0.35318	15:32:29.32	-43:12:02.87	17.360	0.003	0.630	0.007
V445	EcB	∼11.49	15:32:30.19	-43:08:59.26	20.147	0.015	1.191	0.018
V446	EcB	0.65738	15:32:30.51	-43:06:51.95	20.223	0.019	1.137	0.022
V449	EcB	∼7.69	15:32:32.17	-43:08:53.59	20.544	0.020	0.580	0.028
V451	W UMa	0.24724	15:32:34.48	-42:57:09.15	18.203	0.005	0.941	0.006
V452	W UMa	0.33083	15:32:34.63	-42:51:05.65	17.443	0.011	0.611	0.029
V456	EcB	∼21.28	15:32:35.44	-43:08:53.39	19.110	0.006	1.352	0.008
V458	EcB	∼15.15	15:32:36.48	-43:09:59.90	19.770	0.009	1.006	0.012
V461	EcB	∼1.99	15:32:37.22	-42:58:25.87	20.524	0.040	1.099	0.052
V462	EcB	0.52219	15:32:37.32	-42:48:19.15	19.150	0.011	1.630	0.012
V464	EcB	∼16.39	15:32:39.33	-43:10:51.98	17.055	0.003	0.792	0.006
V467	EcB	0.67979	15:32:39.68	-43:12:29.51	17.295	0.003	0.253	0.004
V469	EcB	∼18.87	15:32:42.66	-43:04:24.40	19.446	0.007	1.226	0.009
V472	EcB	∼3.98	15:32:45.16	-43:15:47.04	14.766	0.010	-	-
V476	EcB	0.58581	15:32:47.97	-43:05:49.23	16.854	0.015	0.466	0.027
V477	EcB	0.42723	15:32:48.11	-43:04:12.88	19.915	0.014	1.218	0.022
V480	EcB	4.60817	15:32:49.05	-42:33:40.34	19.025	0.006	0.869	0.010
V481	W UMa	0.32570	15:32:49.31	-43:18:29.81	16.516	0.004	0.694	0.009
V483	EcB	3.04153	15:32:51.00	-42:43:25.24	19.447	0.014	0.946	0.017
V492	W UMa	0.32995	15:32:58.43	-43:05:21.34	16.495	0.003	0.793	0.006
V494	W UMa	0.27502	15:33:00.05	-43:14:27.23	18.767	0.007	0.926	0.010
V29	'AB' RR Lyr	0.72284	15:28:44.53	-43:11:26.93	15.202	0.003	0.432	0.011
V48	'C' RR Lyr	0.29914	15:28:58.14	-43:11:59.12	15.663	0.002	0.221	0.005
V247	'AB' RR Lyr	0.55755	15:31:00.05	-43:13:53.02	15.507	0.002	0.503	0.013
V387	'AB' RR Lyr	0.57167	15:32:00.03	-43:18:41.70	17.746	0.005	0.447	0.007
V221	δ Scuti	0.044967	15:30:34.59	-43:06:53.39	17.413	0.003	0.318	0.006

ID	Type	Period (d)	RA (j2000.0) h m s	DEC (j2000.0) ° ′ ″	V	σV	V-I	σ(V-I)
V270	δ Scuti	0.089530	15:31:07.03	-43:12:07.56	16.615	0.005	0.289	0.011
V283	δ Scuti	0.052169	15:31:12.45	-43:01:49.96	18.045	0.004	0.282	0.007
V284	δ Scuti	0.051600	15:31:12.82	-42:40:10.26	17.065	0.003	0.343	0.005
V293	δ Scuti	0.057857	15:31:16.88	-42:33:54.16	15.974	0.002	0.304	0.004
V322	δ Scuti	0.039243	15:31:28.95	-42:48:36.66	17.665	0.007	0.555	0.014
V324	δ Scuti	0.079601	15:31:29.54	-43:00:00.51	17.416	0.004	0.305	0.006
V340	δ Scuti	0.033293	15:31:37.84	-43:17:28.86	17.376	0.008	0.263	0.014
V457	δ Scuti	0.057240	15:32:35.72	-42:55:55.97	17.730	0.005	0.336	0.006
V459	δ Scuti	0.003919	15:32:36.67	-42:32:21.98	16.017	0.002	0.427	0.003
V482	δ Scuti	0.055329	15:32:49.79	-42:36:31.65	16.082	0.003	0.401	0.004
V5	puls	0.82803*	15:28:33.09	-43:13:09.05	19.163	0.008	1.040	0.011
V27	puls	0.53613*	15:28:43.37	-43:19:32.32	19.792	0.011	1.311	0.014
V39	puls	0.56404	15:28:50.40	-42:36:22.60	19.135	0.006	1.610	0.016
V50	puls	0.24001*	15:29:00.16	-42:38:27.33	17.303	0.011	0.391	0.019
V70	puls	0.49530	15:29:11.40	-43:19:47.48	16.556	0.003	0.811	0.004
V71	puls	0.76145*	15:29:13.02	-42:38:57.31	18.734	0.007	1.842	0.008
V73	puls	1.79230	15:29:13.64	-42:58:51.54	17.395	0.003	0.867	0.004
V80	puls	$\sim$1.23680	15:29:16.25	-43:05:25.57	17.635	0.003	1.287	0.004
V85	puls	1.60200	15:29:16.98	-42:41:11.50	18.213	0.006	1.478	0.007
V95	puls	0.72780	15:29:23.21	-43:14:25.19	18.693	0.006	1.083	0.008
V100	puls	0.27869*	15:29:26.76	-43:13:59.07	17.250	0.012	0.469	0.016
V102	puls	0.58834	15:29:27.90	-43:04:49.08	19.647	0.011	1.111	0.014
V104	puls	0.88471	15:29:29.65	-43:14:52.35	19.104	0.007	1.157	0.008
V124	puls	1.50118	15:29:43.01	-42:37:06.05	18.490	0.006	2.185	0.007
V137	puls	0.86994	15:29:46.86	-42:38:09.34	17.432	0.004	1.322	0.005
V140	puls	1.39000	15:29:49.34	-42:38:15.44	16.091	0.004	-	-
V162	puls	0.87648	15:30:02.71	-42:35:11.54	20.541	0.022	1.454	0.026
V195	puls	0.34534	15:30:18.18	-42:56:41.78	18.080	0.004	1.291	0.009
V202	puls	0.71040	15:30:21.43	-42:34:09.06	20.981	0.031	2.851	0.032
V214	puls	0.52975	15:30:31.73	-42:33:25.43	19.644	0.012	1.366	0.014
V217	puls	0.24462	15:30:32.63	-42:39:28.83	20.391	0.016	1.480	0.019
V238	puls	0.12377*	15:30:54.67	-42:59:57.20	18.462	0.004	0.819	0.006
V244	puls	0.70080	15:30:58.27	-42:44:28.24	17.845	0.008	1.414	0.011
V249	puls	1.78940	15:31:00.92	-42:31:14.49	17.138	0.003	0.779	0.004
V278	puls	1.99370	15:31:09.73	-42:47:30.38	17.206	0.006	0.819	0.008
V280	puls	1.28910	15:31:10.86	-43:02:24.79	18.778	0.006	0.797	0.007
V290	puls	0.95801	15:31:14.65	-42:32:07.28	16.997	0.010	1.133	0.013
V291	puls	0.26803	15:31:15.06	-42:30:39.15	16.279	0.003	0.333	0.004
V295	puls	0.04159	15:31:18.06	-42:54:01.72	17.613	0.006	0.932	0.008
V303	puls	1.16566	15:31:20.98	-42:32:34.73	19.615	0.012	1.558	0.014
V308	puls	0.85152	15:31:23.53	-42:50:14.70	20.208	0.022	1.129	0.026
V313	puls	1.51155	15:31:24.63	-43:02:17.25	16.690	0.003	0.731	0.006
V319	puls	0.31448	15:31:26.82	-43:08:55.28	18.996	0.006	0.279	0.011
V331	puls	1.82460	15:31:35.11	-42:30:24.27	18.075	0.003	0.735	0.004
V338	puls	1.68400	15:31:37.62	-42:36:38.57	17.350	0.002	0.445	0.004
V353	puls	0.91219	15:31:45.92	-42:35:26.45	19.262	0.008	1.081	0.010
V358	puls	0.91176	15:31:46.60	-43:10:18.86	18.753	0.014	0.841	0.021
V372	puls	0.22507	15:31:53.15	-43:13:25.81	20.192	0.022	3.508	0.022
V373	puls	0.58767	15:31:53.69	-43:06:52.28	17.383	0.005	0.778	0.007

ID	Type	Period (d)	RA (j2000.0) h m s	DEC (j2000.0) ° ′ ″	V	σV	V-I	σ(V-I)
V376	puls	1.07188	15:31:55.27	-42:32:40.72	19.282	0.008	1.489	0.009
V391	puls	?	15:32:03.91	-42:51:13.84	14.793	0.009	-	-
V397	puls	0.87095*	15:32:06.43	-42:58:02.41	15.720	0.003	0.602	0.005
V406	puls	1.53755	15:32:10.97	-42:46:01.58	18.827	0.007	1.054	0.009
V432	puls	0.21786	15:32:24.34	-42:31:19.05	18.964	0.007	1.115	0.009
V434	puls	0.21786	15:32:25.26	-42:30:48.94	19.226	0.016	0.700	0.023
V443	puls	0.62793	15:32:29.26	-43:14:18.54	21.011	0.029	1.567	0.033
V448	puls	1.54900	15:32:30.96	-43:02:02.54	18.491	0.007	1.210	0.008
V453	puls	∼0.16550	15:32:34.81	-42:51:04.92	17.589	0.012	1.623	0.013
V454	puls	1.34368	15:32:34.91	-42:47:40.11	18.169	0.007	0.700	0.009
V489	puls	1.00150	15:32:56.86	-43:00:09.43	17.864	0.007	0.755	0.024
V491	puls	∼0.20061	15:32:58.17	-42:52:13.77	14.844	0.007	0.365	0.012
V1	LPV	21.28	15:28:29.26	-43:11:53.40	21.035	0.057	0.993	0.069
V6	LPV	10.30	15:28:33.72	-43:02:05.83	16.299	0.003	1.017	0.005
V7	LPV	∼22.73	15:28:33.85	-43:07:08.89	17.025	0.004	0.850	0.005
V9	LPV	∼17.33	15:28:34.50	-43:17:58.58	16.618	0.007	0.911	0.009
V11	LPV	4.0984	15:28:36.06	-42:57:18.28	16.732	0.003	1.037	0.005
V12	LPV	∼19.23	15:28:37.54	-43:07:40.62	15.984	0.004	0.686	0.007
V13	LPV	6.875	15:28:38.25	-42:37:39.37	15.910	0.002	0.739	0.004
V14	LPV	4.01	15:28:38.70	-43:04:08.15	17.997	0.003	0.694	0.005
V16	LPV	2.6865	15:28:39.31	-43:07:00.16	18.679	0.005	0.756	0.007
V18	LPV	6.63	15:28:40.72	-43:03:23.26	18.666	0.005	2.115	0.005
V19	LPV	2.0388	15:28:41.04	-42:32:21.15	17.947	0.004	1.182	0.006
V21	LPV	3.3229	15:28:41.54	-43:13:17.50	16.614	0.003	0.650	0.004
V22	LPV	2.7833	15:28:41.84	-43:14:16.86	18.479	0.012	1.265	0.015
V23	LPV	14.95	15:28:42.35	-43:02:11.09	17.730	0.003	0.717	0.004
V25	LPV	16.58	15:28:42.98	-42:58:19.01	17.476	0.004	1.087	0.004
V33	LPV	3.923	15:28:46.88	-43:03:26.91	18.403	0.007	1.030	0.011
V34	LPV	12.92	15:28:47.61	-42:38:04.46	17.929	0.004	1.751	0.006
V35	LPV	7.4	15:28:47.71	-43:19:31.44	16.910	0.005	0.871	0.006
V38	LPV	7.22	15:28:50.06	-43:10:03.62	17.598	0.003	1.141	0.004
V40	LPV	13.87	15:28:50.51	-43:13:16.34	16.457	0.003	0.729	0.004
V45	LPV	7.13	15:28:55.18	-42:37:15.81	18.109	0.004	1.311	0.007
V47	LPV	5.93	15:28:57.79	-43:04:26.36	18.242	0.005	0.840	0.007
V52	LPV	15.72	15:29:00.46	-43:04:46.56	18.559	0.005	1.876	0.007
V53	LPV	∼4.133	15:29:00.51	-42:57:17.27	16.041	0.002	0.696	0.004
V54	LPV	12.61	15:29:00.75	-42:32:19.27	16.550	0.002	0.771	0.003
V55	LPV	4.249	15:29:01.43	-43:02:27.74	16.398	0.002	0.633	0.004
V56	LPV	4.156	15:29:01.98	-43:15:52.40	19.618	0.009	1.253	0.011
V57	LPV	15.10	15:29:02.53	-43:12:12.23	15.319	0.003	0.685	0.018
V63	LPV	∼4.20	15:29:06.86	-43:13:31.45	18.098	0.031	1.352	0.039
V64	LPV	∼18.87	15:29:08.82	-43:06:05.73	16.803	0.003	0.754	0.005
V67	LPV	5.37	15:29:09.23	-43:13:16.71	19.050	0.007	1.744	0.008
V68	LPV	∼18.38	15:29:10.47	-42:57:44.81	17.866	0.003	1.046	0.004
V69	LPV	5.4065	15:29:10.82	-42:57:15.10	18.358	0.004	1.481	0.005
V72	LPV	∼18.90	15:29:13.57	-43:00:10.78	16.256	0.002	0.870	0.004
V74	LPV	8.197	15:29:13.77	-42:41:26.58	18.157	0.006	0.914	0.007
V75	LPV	3.172	15:29:14.49	-43:07:24.41	16.821	0.003	0.824	0.005
V77	LPV	7.943	15:29:14.89	-42:38:49.80	17.904	0.003	1.108	0.005
V78	LPV	4.19	15:29:15.67	-43:11:06.82	17.139	0.002	0.699	0.004

ID	Type	Period (d)	RA (j2000.0) h m s	DEC (j2000.0) ° ′ ″	V	σV	V-I	σ(V-I)
V81	LPV	4.625	15:29:16.26	-42:34:05.06	17.227	0.003	0.826	0.004
V82	LPV	3.580	15:29:16.45	-42:31:40.20	17.725	0.003	1.048	0.004
V86	LPV	∼14.70	15:29:17.21	-42:58:44.07	17.695	0.006	1.434	0.010
V87	LPV	14.81	15:29:17.49	-42:57:06.98	16.572	0.004	0.964	0.006
V88	LPV	∼11.24	15:29:17.70	-42:39:15.39	16.256	0.003	0.703	0.005
V89	LPV	8.289	15:29:19.68	-43:05:37.62	16.077	0.003	0.843	0.006
V90	LPV	9.13	15:29:20.11	-43:16:01.66	19.108	0.008	1.367	0.009
V93	LPV	4.543	15:29:21.00	-43:06:22.37	19.598	0.011	1.459	0.013
V96	LPV	16.39	15:29:23.49	-43:01:02.69	16.448	0.002	0.703	0.004
V97	LPV	∼21.28	15:29:23.61	-42:39:09.07	17.561	0.003	0.774	0.005
V98	LPV	5.848	15:29:24.95	-43:07:06.98	17.350	0.003	0.705	0.005
V99	LPV	∼21.74	15:29:26.05	-43:18:30.03	17.020	0.003	0.960	0.005
V101	LPV	14.28	15:29:27.28	-42:58:07.87	15.906	0.002	0.814	0.010
V103	LPV	8.816	15:29:29.23	-43:00:59.20	17.441	0.004	0.799	0.006
V105	LPV	8.98	15:29:30.07	-43:13:26.23	17.150	0.004	0.833	0.006
V108	LPV	8.474	15:29:30.89	-43:14:41.31	16.787	0.002	0.669	0.004
V109	LPV	38.66	15:29:34.14	-42:56:24.65	15.247	0.004	-	-
V110	LPV	∼18.87	15:29:34.91	-43:11:31.86	15.741	0.004	1.008	0.011
V112	LPV	9.584	15:29:36.70	-42:30:02.18	16.992	0.003	0.916	0.004
V116	LPV	∼25.00	15:29:39.60	-42:30:09.04	15.860	0.002	0.863	0.004
V119	LPV	20.0	15:29:41.62	-43:06:06.86	17.786	0.005	1.099	0.007
V120	LPV	13.26	15:29:41.83	-43:00:41.58	17.357	0.002	0.741	0.005
V121	LPV	∼10.99	15:29:42.00	-43:20:03.11	15.999	0.002	0.636	0.006
V122	LPV	3.633	15:29:42.25	-43:01:45.55	18.306	0.006	0.892	0.008
V123	LPV	4.635	15:29:42.81	-42:56:28.33	17.433	0.003	1.004	0.006
V125	LPV	7.626	15:29:43.30	-43:05:57.19	17.032	0.003	0.651	0.006
V126	LPV	5.049	15:29:43.54	-43:01:58.36	17.495	0.003	0.865	0.006
V127	LPV	4.94	15:29:43.96	-43:00:31.74	16.126	0.002	0.770	0.008
V128	LPV	3.765	15:29:44.11	-43:07:20.58	17.272	0.004	0.899	0.006
V129	LPV	∼21.74	15:29:44.55	-43:03:22.63	15.572	0.002	0.695	0.008
V132	LPV	∼21.28	15:29:45.36	-42:33:53.01	17.222	0.002	0.734	0.004
V133	LPV	∼21.74	15:29:45.59	-42:37:18.88	17.024	0.004	0.977	0.006
V135	LPV	6.90	15:29:46.68	-43:16:19.29	18.390	0.005	0.716	0.006
V136	LPV	23.20	15:29:46.69	-42:40:35.94	14.696	0.006	-	-
V142	LPV	5.502	15:29:49.80	-42:56:14.31	18.756	0.004	1.130	0.008
V143	LPV	4.58	15:29:50.02	-43:16:55.14	18.556	0.005	0.882	0.006
V146	LPV	5.628	15:29:50.61	-43:00:31.50	17.368	0.003	0.797	0.006
V147	LPV	5.691	15:29:51.51	-43:01:56.35	19.497	0.012	1.108	0.016
V148	LPV	∼9.03	15:29:51.74	-43:16:26.38	18.471	0.005	0.806	0.007
V150	LPV	∼18.87	15:29:52.21	-43:18:31.84	18.009	0.029	1.148	0.056
V152	LPV	12.0	15:29:57.04	-43:05:35.49	16.840	0.003	0.865	0.007
V153	LPV	5.76	15:29:57.05	-42:58:32.91	15.335	0.003	-	-
V154	LPV	24.61	15:29:58.15	-43:17:14.60	15.468	0.003	0.727	0.011
V156	LPV	∼7.94	15:29:58.56	-42:33:07.99	17.061	0.002	0.750	0.004
V157	LPV	4.812	15:29:59.17	-43:19:23.88	18.543	0.005	0.916	0.008
V158	LPV	7.411	15:29:59.56	-42:57:25.35	18.849	0.008	0.900	0.012
V159	LPV	6.96	15:30:00.52	-42:59:30.85	17.516	0.003	0.830	0.008
V160	LPV	6.68	15:30:01.77	-42:39:01.15	17.931	0.014	0.770	0.017
V163	LPV	12.73	15:30:03.45	-42:58:23.94	17.173	0.003	1.109	0.009

ID	Type	Period (d)	RA (j2000.0) h m s	DEC (j2000.0) ° ′ ″	V	σV	V-I	σ(V-I)
V164	LPV	9.473	15:30:03.62	-42:30:55.12	17.905	0.004	0.956	0.006
V166	LPV	9.76	15:30:04.72	-42:34:57.34	18.740	0.005	1.018	0.007
V169	LPV	3.237	15:30:07.93	-42:31:48.33	19.234	0.009	1.084	0.011
V173	LPV	∼10.2	15:30:08.67	-42:59:36.41	15.533	0.007	0.783	0.016
V174	LPV	7.29	15:30:09.08	-42:38:06.54	18.854	0.008	1.222	0.009
V175	LPV	9.90	15:30:09.30	-43:00:19.69	15.727	0.003	0.695	0.016
V176	LPV	∼19.23	15:30:10.23	-42:29:58.96	18.020	0.007	0.981	0.009
V177	LPV	14.49	15:30:11.38	-43:02:41.60	16.159	0.004	0.747	0.010
V179	LPV	6.93	15:30:11.80	-42:30:54.07	17.637	0.003	0.692	0.005
V180	LPV	9.54	15:30:13.09	-42:33:48.45	17.103	0.003	1.305	0.007
V182	LPV	5.97	15:30:13.46	-42:34:02.34	20.133	0.012	1.893	0.028
V183	LPV	∼22.73	15:30:13.52	-42:38:37.26	18.175	0.005	1.005	0.006
V185	LPV	7.028	15:30:15.34	-43:11:01.75	18.177	0.005	0.722	0.008
V186	LPV	∼21.28	15:30:15.44	-43:13:05.93	18.175	0.009	1.190	0.010
V187	LPV	∼18.15	15:30:15.86	-42:38:01.83	16.943	0.004	0.843	0.006
V190	LPV	8.42	15:30:17.43	-43:01:07.30	17.023	0.004	0.799	0.007
V191	LPV	11.65	15:30:17.67	-42:33:39.01	20.631	0.024	1.683	0.027
V192	LPV	∼15.63	15:30:18.04	-42:57:17.77	15.889	0.003	0.664	0.016
V193	LPV	4.372	15:30:18.08	-43:14:18.82	17.353	0.003	0.678	0.006
V194	LPV	∼24.39	15:30:18.14	-42:37:14.61	17.007	0.003	0.741	0.006
V197	LPV	∼5.051	15:30:18.74	-43:14:15.42	16.865	0.005	0.779	0.006
V198	LPV	∼11.49	15:30:19.80	-43:09:48.32	15.683	0.003	0.569	0.009
V199	LPV	3.533	15:30:20.49	-43:06:34.09	17.957	0.005	1.323	0.009
V200	LPV	∼22.22	15:30:20.77	-43:11:51.58	16.391	0.002	0.346	0.005
V205	LPV	2.690	15:30:27.36	-43:11:53.31	17.314	0.004	0.783	0.008
V208	LPV	7.862	15:30:28.89	-42:57:33.17	18.841	0.006	0.908	0.009
V209	LPV	11.655	15:30:29.81	-42:30:31.79	19.182	0.005	0.938	0.008
V211	LPV	∼8.265	15:30:31.05	-43:09:24.79	15.285	0.005	-	-
V213	LPV	8.265	15:30:31.49	-42:58:56.27	18.414	0.004	1.100	0.005
V215	LPV	8.380	15:30:31.99	-43:17:04.20	16.039	0.004	0.932	0.012
V216	LPV	3.672	15:30:32.56	-43:06:41.07	18.964	0.016	0.907	0.024
V219	LPV	11.90	15:30:34.28	-43:04:34.58	16.923	0.004	0.979	0.007
V220	LPV	16.06	15:30:34.54	-42:56:18.91	15.912	0.003	0.720	0.011
V222	LPV	2.157	15:30:34.85	-42:59:33.80	19.619	0.011	1.429	0.013
V225	LPV	14.95	15:30:36.70	-43:15:53.27	15.418	0.006	0.780	0.022
V226	LPV	4.604	15:30:37.61	-43:04:28.16	18.828	0.005	1.401	0.008
V227	LPV	5.607	15:30:37.78	-43:13:34.38	16.108	0.004	0.653	0.008
V229	LPV	∼19.61	15:30:50.56	-43:15:07.35	16.297	0.003	0.644	0.008
V230	LPV	5.10	15:30:50.96	-42:50:31.11	17.195	0.008	0.778	0.010
V233	LPV	4.344	15:30:52.44	-43:15:41.16	19.401	0.011	1.162	0.012
V234	LPV	∼21.74	15:30:52.50	-43:20:26.77	17.889	0.004	0.827	0.006
V235	LPV	10.74	15:30:53.22	-43:17:34.47	18.600	0.005	0.799	0.009
V237	LPV	9.60	15:30:54.29	-42:39:09.08	16.098	0.003	0.662	0.006
V239	LPV	18.61	15:30:55.37	-43:06:19.67	17.466	0.015	0.651	0.025
V240	LPV	5.44	15:30:55.44	-42:58:06.47	17.779	0.004	0.767	0.006
V242	LPV	8.064	15:30:57.30	-43:07:23.12	18.372	0.006	1.060	0.009
V245	LPV	∼5.076	15:30:59.23	-43:19:50.79	17.262	0.006	1.535	0.008

ID	Type	Period (d)	RA (j2000.0) h m s	DEC (j2000.0) ° ′ ″	V	σV	V-I	σ(V-I)
V255	LPV	11.62	15:31:02.34	-42:39:19.19	19.645	0.009	1.782	0.011
V256	LPV	8.279	15:31:02.85	-42:38:57.92	18.181	0.009	0.956	0.019
V258	LPV	4.244	15:31:03.08	-42:34:49.00	19.364	0.008	1.034	0.011
V259	LPV	∼2.02	15:31:03.33	-42:53:23.32	-	-	-	-
V260	LPV	∼23.26	15:31:03.83	-42:30:32.35	17.409	0.003	1.110	0.005
V263	LPV	10.68	15:31:05.18	-42:30:47.20	18.857	0.006	2.339	0.007
V265	LPV	17.58	15:31:05.57	-42:40:51.21	18.233	0.027	0.854	0.037
V266	LPV	∼10.87	15:31:05.82	-43:08:50.85	16.353	0.003	0.937	0.005
V267	LPV	∼18.18	15:31:06.04	-43:14:49.65	16.703	0.003	0.787	0.007
V269	LPV	∼15.15	15:31:06.46	-42:36:56.38	15.946	0.002	0.844	0.006
V273	LPV	3.76	15:31:08.18	-43:14:33.15	19.256	0.007	1.008	0.010
V274	LPV	13.39	15:31:08.60	-43:04:49.05	17.329	0.004	0.735	0.006
V275	LPV	9.140	15:31:08.82	-43:00:31.92	18.403	0.010	1.259	0.011
V279	LPV	∼7.430	15:31:10.25	-42:55:51.91	16.386	0.005	0.724	0.006
V282	LPV	8.850	15:31:11.42	-42:52:51.22	16.956	0.005	0.860	0.007
V286	LPV	7.403	15:31:13.34	-42:58:31.08	18.954	0.006	0.761	0.008
V287	LPV	15.11	15:31:13.68	-43:12:27.67	18.527	0.005	1.438	0.006
V289	LPV	7.239	15:31:14.27	-42:31:59.50	18.160	0.005	1.084	0.006
V292	LPV	4.696	15:31:16.76	-43:17:04.43	15.689	0.005	0.660	0.011
V298	LPV	2.495	15:31:19.73	-42:33:30.86	19.122	0.012	1.644	0.019
V299	LPV	9.023	15:31:19.74	-42:57:18.36	18.225	0.005	0.777	0.007
V300	LPV	7.370	15:31:20.32	-42:52:18.13	16.084	0.005	0.719	0.006
V301	LPV	∼18.519	15:31:20.38	-43:13:45.95	18.989	0.007	0.745	0.011
V309	LPV	2.036	15:31:23.75	-43:12:25.97	17.868	0.004	1.151	0.006
V311	LPV	16.05	15:31:23.83	-42:44:30.76	17.578	0.006	1.036	0.009
V314	LPV	6.029	15:31:24.82	-42:40:01.30	17.417	0.004	0.977	0.006
V315	LPV	4.024	15:31:25.00	-42:51:32.36	16.598	0.005	0.809	0.006
V316	LPV	16.10	15:31:25.19	-42:47:06.86	18.696	0.026	1.193	0.043
V318	LPV	2.746	15:31:26.16	-42:29:50.65	16.776	0.002	0.851	0.004
V320	LPV	∼24.39	15:31:27.01	-42:36:50.50	18.609	0.005	1.981	0.006
V321	LPV	7.79	15:31:27.47	-42:50:27.26	17.666	0.006	0.860	0.009
V323	LPV	4.34	15:31:29.14	-43:19:55.83	18.399	0.005	0.839	0.007
V325	LPV	6.917	15:31:30.25	-42:39:06.38	16.246	0.054	0.953	0.054
V326	LPV	6.79	15:31:30.76	-43:16:53.56	17.712	0.008	0.644	0.011
V327	LPV	6.81	15:31:30.86	-43:16:55.69	18.641	0.021	0.566	0.028
V328	LPV	3.853	15:31:31.35	-42:33:20.86	19.059	0.006	1.015	0.009
V329	LPV	9.58	15:31:33.46	-43:19:23.48	19.135	0.011	0.585	0.014
V332	LPV	23.20	15:31:35.22	-43:12:28.03	20.490	0.072	0.558	0.088
V335	LPV	3.2955	15:31:37.20	-42:43:50.62	17.170	0.007	0.826	0.015
V341	LPV	∼23.26	15:31:38.47	-42:50:15.44	16.249	0.003	0.812	0.005
V343	LPV	3.647	15:31:38.97	-42:29:36.15	17.722	0.004	1.430	0.005
V346	LPV	6.329	15:31:42.00	-42:32:28.47	18.908	0.006	0.968	0.009
V348	LPV	2.202	15:31:43.03	-43:09:49.22	18.350	0.003	1.075	0.006
V349	LPV	2.310	15:31:43.12	-42:37:34.64	18.349	0.005	1.603	0.006
V350	LPV	∼21.74	15:31:43.55	-43:15:40.75	17.865	0.004	0.649	0.008
V357	LPV	13.19	15:31:46.52	-42:30:38.86	18.336	0.007	0.768	0.011
V360	LPV	13.90	15:31:47.62	-43:12:18.67	17.943	0.017	1.268	0.026
V361	LPV	21.75	15:31:47.73	-43:12:57.97	16.451	0.002	0.760	0.006
V362	LPV	17.31	15:31:48.88	-43:13:58.33	15.969	0.002	0.653	0.004

ID	Type	Period (d)	RA (j2000.0) h m s	DEC (j2000.0) ° ′ ″	V	σV	V-I	σ(V-I)
V364	LPV	7.183	15:31:50.64	-43:15:33.98	19.242	0.013	2.031	0.014
V370	LPV	3.916	15:31:52.09	-42:51:34.77	17.090	0.007	0.815	0.009
V375	LPV	5.916	15:31:54.82	-42:36:09.20	19.327	0.010	1.665	0.011
V377	LPV	8.282	15:31:55.78	-43:02:13.09	18.291	0.004	0.884	0.006
V379	LPV	31.00	15:31:56.58	-43:06:35.71	14.847	0.008	-	-
V380	LPV	4.431	15:31:56.78	-43:00:03.54	19.757	0.012	1.131	0.014
V382	LPV	21.74	15:31:57.59	-42:53:10.59	14.406	0.012	-	-
V384	LPV	7.911	15:31:58.55	-43:04:09.71	19.561	0.012	1.228	0.014
V386	LPV	4.922	15:31:59.54	-43:04:16.24	16.826	0.017	0.769	0.023
V388	LPV	6.328	15:32:00.25	-43:16:32.92	18.569	0.005	0.817	0.006
V389	LPV	6.577	15:32:03.19	-43:15:36.28	19.218	0.008	0.846	0.014
V390	LPV	9.843	15:32:03.59	-42:31:57.77	17.897	0.003	0.832	0.005
V392	LPV	14.39	15:32:03.92	-42:45:57.27	17.061	0.005	1.184	0.006
V394	LPV	14.11	15:32:05.53	-42:59:39.29	18.574	0.025	1.658	0.027
V396	LPV	6.996	15:32:06.29	-43:17:28.12	15.664	0.001	-1.849	0.016
V398	LPV	6.602	15:32:06.52	-43:17:30.54	18.163	0.021	0.650	0.026
V401	LPV	∼9.08	15:32:07.63	-43:15:44.87	17.677	0.003	0.308	0.005
V407	LPV	3.398	15:32:11.18	-42:32:18.10	17.209	0.002	1.314	0.004
V408	LPV	9.35	15:32:11.25	-43:19:17.71	16.726	0.003	0.759	0.004
V409	LPV	10.95	15:32:12.28	-42:31:43.23	14.979	0.004	-	-
V412	LPV	∼2.364	15:32:15.43	-42:59:21.73	18.557	0.008	1.201	0.011
V414	LPV	∼3.984	15:32:16.05	-42:53:12.41	18.563	0.006	1.134	0.008
V415	LPV	18.89	15:32:17.39	-43:16:06.34	16.825	0.003	1.002	0.006
V417	LPV	9.12	15:32:18.21	-42:53:09.06	19.535	0.013	2.234	0.014
V420	LPV	7.307	15:32:19.20	-42:36:59.71	17.591	0.005	0.778	0.006
V421	LPV	2.4611	15:32:19.45	-43:11:46.24	17.894	0.003	0.693	0.005
V423	LPV	15.395	15:32:20.27	-42:42:53.41	18.853	0.008	1.077	0.014
V425	LPV	5.799	15:32:21.73	-43:09:32.51	17.722	0.003	0.704	0.006
V427	LPV	10.04	15:32:23.17	-42:37:03.14	18.129	0.011	1.120	0.012
V436	LPV	7.40	15:32:25.57	-43:12:05.03	17.490	0.002	0.790	0.004
V439	LPV	9.78	15:32:28.64	-43:01:31.67	16.585	0.002	0.669	0.004
V440	LPV	6.30	15:32:28.80	-42:57:02.91	17.978	0.004	0.898	0.006
V447	LPV	7.319	15:32:30.81	-42:39:33.69	19.734	0.013	1.127	0.016
V450	LPV	∼4.88	15:32:32.80	-43:18:14.46	18.106	0.004	2.023	0.006
V455	LPV	8.665	15:32:35.39	-43:02:01.63	18.213	0.004	1.000	0.006
V460	LPV	21.40	15:32:36.69	-42:56:21.76	18.761	0.007	2.719	0.008
V463	LPV	6.551	15:32:37.37	-43:09:54.35	19.994	0.014	1.069	0.017
V465	LPV	10.22	15:32:39.58	-42:39:37.19	17.823	0.003	1.069	0.005
V466	LPV	10.66	15:32:39.60	-42:48:02.25	18.194	0.016	0.969	0.022
V468	LPV	10.32	15:32:40.96	-42:31:23.08	20.099	0.015	1.466	0.017
V470	LPV	5.01	15:32:42.84	-43:06:04.83	17.263	0.004	0.616	0.007
V471	LPV	8.92	15:32:45.15	-43:18:08.79	17.662	0.005	0.749	0.008
V473	LPV	4.80	15:32:45.51	-43:16:44.77	17.343	0.004	0.998	0.006
V474	LPV	12.60	15:32:45.68	-42:47:48.89	15.892	0.004	0.825	0.006
V475	LPV	9.96	15:32:46.57	-43:03:30.21	14.799	0.010	-	-
V478	LPV	∼21.28	15:32:48.17	-42:31:57.88	18.660	0.005	1.312	0.007
V479	LPV	13.38	15:32:48.49	-42:52:14.25	18.404	0.006	0.916	0.008
ID	Type	Period (d)	RA (j2000.0) h m s	DEC (j2000.0) ° ′ ″	V	σV	V-I	σ(V-I)
V484	LPV	∼22.22	15:32:52.17	-43:14:19.93	14.757	0.010	-	-
V485	LPV	4.984	15:32:53.44	-42:42:25.61	18.586	0.006	1.646	0.008
V486	LPV	6.44	15:32:55.40	-43:04:04.95	17.671	0.004	0.699	0.007
V487	LPV	12.50	15:32:55.49	-42:44:05.71	16.495	0.006	1.156	0.009
V488	LPV	∼23.26	15:32:55.98	-43:05:08.96	16.850	0.003	1.050	0.007
V490	LPV	9.77	15:32:57.22	-43:16:03.09	17.690	0.005	0.697	0.009
V493	LPV	5.279	15:32:58.45	-43:02:20.01	15.956	0.002	0.615	0.006
V134	Irr	?	15:29:45.87	-42:55:56.57	16.647	0.003	0.349	0.006

Table 2: Table of all detected variable stars in our Lupus field. Tabulated are the variable star identification number, the type of variable, the period, RA and DEC (given in J2000.0), V magnitude, V error, V−I color and its associated uncertainty. Those pulsators with periods marked as $*$ are those which could be eclipsing binaries with twice the tabulated period. Unknown magnitude values are marked as '−'